



universität
wien

DIPLOMARBEIT

Heterogeneous *MYCN* amplification in neuroblastoma
- amplicon, genomic background and genome instability -

angestrebter akademischer Grad

Magister der Naturwissenschaften (Mag. rer.nat.)

Verfasser: Dominik Bogen
Matrikelnummer: 0405928
Studienrichtung /Studienzweig A490
(lt. Studienblatt):

Betreuerin / Betreuer: Hans Rotheneder, PhD, M.Sc.

Wien, im Mai 2010

Kurzfassung

Unter den 110 *MYCN* amplifizierten (MNA) Neuroblastomen, die in den letzten 10 Jahren am CCRI analysiert wurden, befanden sich 26 Tumore mit variierender Anzahl von Tumorzellen oder Arealen ohne MNA. In Übereinstimmung mit den Richtlinien der INRG Biologie Gruppe wurden diese Tumore als „heterogen *MYCN*- amplifiziert (hetMNA)“ eingestuft. Da der genomische Hintergrund von hetMNA- Tumoren bis jetzt noch nicht beschrieben wurde, versuchten wir Gemeinsamkeiten in segmentalen und/oder numerischen Aberrationen (SCA und/oder NCA) zu finden. Von bis zu vier Tumorstücken vom selben hetMNA Tumor von fünf Patienten wurden Kryoschnitte angefertigt. Insgesamt wurden 13 Stücke mit Interphase FISH (I-FISH) analysiert und ihre DNA zur Aufklärung des genomischen Hintergrunds in hetMNA Tumoren mit MLPA und SNP Arrays untersucht. *MYCN*-Heterogenität wurde mit I-FISH detektiert und in Kombination mit der *DDX1*-Sonde angewendet um die Amplikonzusammensetzung festzustellen. γ H2AX- Färbung mit anschließende *MYCN* FISH wurde durchgeführt um das Auftreten von DNA-Doppelstrangbrüchen mit MNA zu korrelieren. Die Quantifizierung der Signale auf den Schnitten wurde mit einem automatischen Aufnahmesystem durchgeführt. Alle analysierten hetMNA-Tumore zeigten NCAs, wobei zwei Proben von je zwei Patienten nur NCAs zeigten, sechs Stücke von vier Tumoren zweier weiteren Patienten wiesen zusätzlich unterschiedliche SCAs auf. Drei von vier Stücken von einem Patienten zeigten ebenfalls nur NCAs, das vierte eine SCA. Zahlreiche Chromosomen waren überrepräsentiert. MNA wurde in je einem Tumorstück von vier Patienten mit MLPA und/oder SNP Arrays bestätigt, während der fünfte MNA nur mit *MYCN*-FISH zeigte. In einem Tumor wurde Heterogenität in der Amplikonzusammensetzung bewiesen und ein anderer zeigte zwei unterschiedliche 1p-Bruchstellen in vier Stücken. Das Muster der γ H2AX-Färbung korrelierte bedingt mit MNA-Tumorzellen. Unsere Daten belegten die Existenz von mehreren Tumorzellklonen und zum Teil unterschiedlichen Amplikons im gleichen Tumor. Mit der angewendeten Auflösung konnte jedoch keine SCA-Gemeinsamkeit gefunden werden, welche MNA bedingen könnte. Es konnten keine eindeutigen Rückschlüsse gezogen werden, dass genomische Instabilität MNA auslöst. Wir können die Notwendigkeit einer detaillierten Tumoraufarbeitung mit I-FISH und DNA-basierenden Techniken, wie sie von der International Neuroblastoma Research Group (INRG) Biology Group vorgeschlagen wird, nur bestätigen, um Heterogenität festzustellen.

Abstract

Among 110 *MYCN* amplified neuroblastomas analyzed at the CCRI in the last decade, 26 tumors contained a varying number of tumor cells/areas without MNA, defined as heterogeneous *MYCN* amplification (hetMNA) according to INRG biology guidelines. Since the genomic background of hetMNA tumors has not yet been described, we looked for common segmental and/or numerical chromosome aberrations and genetic instability as initiators for amplicon formation. Up to four tumor pieces of the same hetMNA tumor from five patients were cryosectioned. In total, thirteen pieces were analyzed by I-FISH and their DNA was analyzed by MLPA and 250k SNP arrays to investigate the genomic background of hetMNA tumors. *MYCN* I-FISH was performed to detect *MYCN* heterogeneity and combined with *DDXI* probes to assess the amplicon composition. γ H2AX staining and subsequent *MYCN* FISH was performed to correlate DNA double strand breaks occurrence with MNA. Quantification of signals on the sections was done with an automatic device. All analyzed hetMNA tumors showed NCAs, two samples from two patients each showed only NCAs; six pieces from four tumors from two patients displayed a variety of inconsistent, additional SCAs. Three of four pieces from one tumor had only NCAs, the fourth one SCA. Numerous chromosomes were unitarily found overrepresented. MNA was confirmed in four tumor pieces of four patients by MLPA/SNP arrays, the fifth showed MNA only in its *MYCN* FISH results. One tumor revealed different amplicon compositions in the same piece and another showed two 1p-breakpoints in four pieces. γ H2AX staining pattern only partially correlated with MNA cells. Our data indicates the existence of multiple tumor cell clones and different amplicons in single hetMNA NBs. At the applied resolution, no common SCA is found to be underlying MNA not excluding subtle genomic changes and mutations. A conclusion on genetic instability as a cause for MNA is premature. Our data strongly supports a detailed tumor work up and the application of both I-FISH and DNA-based techniques as recommended by the INRG.

Table of content

Kurzfassung.....	3
Abstract	5
Table of content.....	7
1 Introduction.....	9
1.1 Neuroblastoma – a pediatric tumor	9
1.2 <i>MYCN</i> amplification in aggressive neuroblastoma	10
1.3 Intratumoral heterogeneity in neuroblastoma.....	13
1.4 Genetic instability in cancer	14
1.5 DNA double strand break response and the histone H2AX	16
1.6 Neuroblastoma, genomic instability and DSB detection.....	18
2 Patients, Materials and Methods	20
2.1 Patients.....	20
2.2 Microscopic techniques	21
2.2.1 Preparation of frozen patient material	21
2.2.2 Histochemistry of frozen sections	21
2.2.3 DNA probe labeling by nick translation for FISH	22
2.2.4 Two-color interphase fluorescent in situ hybridization.....	23
2.2.5 γ H2AX immunohistochemistry on cryosections.....	24
2.2.6 <i>MYCN</i> I-FISH on γ H2AX- prestained tumor sections.....	25
2.3 Genomic evaluations of tumor samples.....	26
2.3.1 DNA extraction from tumor samples	26
2.3.2 Multiplex ligation-dependent probe amplification (MLPA)	26
2.3.3 Single nucleotide polymorphism (SNP) array	28
2.4 Buffers and Solution	29

3	Results.....	31
3.1	Detecting <i>MYCN</i> - heterogeneity in neuroblastoma	31
3.1.1	Hematoxylin and Eosin stainings help in estimating tumor cell content but FISH is needed for detecting tumor heterogeneity	31
3.1.2	Comparison of two-color <i>MYCN</i> I-FISH, MLPA and SNP array analysis for the detection of <i>MYCN</i> heterogeneity in neuroblastoma	33
3.1.3	Intratumoral heterogeneity in <i>MYCN</i> amplicon composition	37
3.2	Genetic heterogeneity in hetMNA neuroblastoma	39
3.3	Genetic instability involvement in <i>MYCN</i> - amplification	48
4	Discussion	54
4.1	Detecting heterogeneity in neuroblastoma	54
4.2	Heterogeneity in amplicon composition.....	56
4.3	Genetic background in hetMNA neuroblastoma	57
4.4	Genetic instability in neuroblastoma	59
5	List of Abbreviations	62
6	List of Figures	63
7	List of Tables	66
8	Reference	67
	Curriculum Vitae.....	74
	Acknowledgements	75

1 Introduction

1.1 Neuroblastoma – a pediatric tumor

Neuroblastoma is a solid form of cancer developing in the extracranial nervous tissue. As a common pediatric tumor with 6-10% of all reported cancer cases in children, its onset timed during early childhood but may already occur prenatally. Neuroblasts originating from the neural crest are the common progenitors of the sympathetic nervous system and the major component of NB tumors. Migration during embryonic development leads to a spread of this cell type which also reflects the pattern of the latter development of the primary disease and the multiple locations NB tumors can be found in [1]. The abdominal cavity with adrenal (40%) and paraspinal ganglia (25%) is the most frequent primary location of the tumor commonly detected in older children. Other initial sites are thorax (15%) and cervix (3%) predominantly found in infants. Pelvis (5%) and miscellaneous sites (12%) add to the diversity of the primary tumor locations.

NB is a heterogeneous disease which largely affects therapy protocol and correlates with the prognosis for recovery of the patient. The severity of the disease is assessed in the different risk categories low, intermediate, and high, which are set up by the International Neuroblastoma Staging System [2]. The severity and the clinical progression of NB can vary from spontaneous regression [3] and maturation [4] to aggressive malignant behavior. Recent findings suggest different emergence and molecular characteristics for tumors in the three different categories. Genomic imbalances occur either sequentially or simultaneously and are considered to be responsible for the heterogeneity of NB [5] and its clinical outcome. Tumors with the best prognosis and a chance of spontaneous regression in the low-risk category showed a hyperdiploid or near-triploid karyotype with whole-chromosome gains but without structural aberrations [5-7]. Near-triploid NBs are frequently associated with a localized phenotype of the tumor, lack of chromosomal structural alterations, and are diagnosed mostly in children of younger age [8]. Structural genomic aberrations of chromosomes usually correspond to a dismal prognosis and characterize the high-risk group. Tumors from children older than 18 month often belong to this category. Amplification of the proto-oncogene *MYCN* and the loss of the short p-arm of chromosome 1 (1p) are frequently occurring patterns in aggressive NB [9]. Loss of heterozygosity (LOH) of other segments like the short arm of

chromosome 3 (3p) and the long q-arm of chromosome 11 (11q), as well as gain 17q are also common contributors to an often fatal course of the disease in high-risk patients [6, 10-12]. A few alterations are frequently present in combination and determine a genetic subset of neuroblastoma. Segmental aberrations at 3p, 11q and 14q pose an example for such a collocation, which seems to be mutually exclusive of 1p-gain and *MYCN* amplification in a different subset [13]. Analyses showed that the pattern of structural changes usually develops sequentially but source and trigger need further investigation [5, 14 (in press)]. To complicate the search, NB is considered to be a sporadic form of cancer given that only a few hereditary cases are reported [15].

1.2 *MYCN* amplification in aggressive neuroblastoma

MYCN is a member of the *MYC*-family of transcription factors and maps to chromosome 2 at 2p23-24 as demonstrated in human neuroblastoma cell lines [16]. The protein is a basic helix-loop-helix (bHLH) protein with the ability to bind DNA through dimerization. The proto-oncogene was first characterized through its amplification in human NB cells [17, 18] with a presence in approximately 23% of the investigated tumors. Normal expression of the gene is relevant in undifferentiated cell types during mammalian embryonic development [19, 20]. *MYCN*, when amplified in postnatal cells, gained further significance as a clinical indicator for an aggressive form of NB with a poor prognosis for survival [21]. Additionally, the amplification of the gene was found in other tumors of neuronal nature including small cell lung cancer (SCLC), retinoblastoma, malignant glioblastoma, and peripheral neuroectodermal tumors (PNET)s [22-25]. *MYCN* is overexpressed in all these tumors. Mutations in the coding region of *MYCN* were not detected by DNA sequence analysis and can thus be excluded as a potential cause for the elevated gene expression contributing to tumorigenesis [26, 27]. In fact, the copy number amplification of up to 250-fold common in neuronal tumors is the reason for the cancerogenous property of *MYCN*.

Amplification of DNA fragments and oncogenes, in particular, can be manifested as intrachromosomal homologous staining regions (hsr) or episomal double minutes (dmin). Both forms are considered to arise after DNA double-strand breakage and permitted by

erroneous DNA repair and non-functional cell cycle checkpoints. Intrachromosomal recombination [28], telomere fusion subsequent to double chromatid breakage at fragile sites [29, 30], or unequal sister chromatid exchanges accompanied by secondary rearrangements can result in short to large tandem duplications at locations close to the single-copy of the wild-type gene. Alternatively, amplification can take place at distant regions from the locus of the single-copy gene after reintegration of episomal DNA [31]. The most popular model for intrachromosomal amplification, however, is the breakage-fusion-bridge cycle which can be found in a number of solid tumors like prostate cancer, osteosarcoma, and squamous cell carcinomas [32-34]. Ultimately, multiple cycles lead to an amplification of genes adjacent to the breakage site which can result in both hsr- and dmin-formation. The amplified sequence is retained at its original chromosomal location. A different explanatory approach is the “episomal model” [35-37]. The target sequence is excised from the chromosome, circularized, and amplified subsequently producing dmin. Excision often leads to the deletion of the single-copy at its normal position in the chromosome. Evidence for this model has been reported, for instance, in cases of acute myeloid leukemia [38].

Support for both theories was also found in case of *MYCN* amplification in neuroblastoma. In addition to the retention of the single-copy at the original position, examined cell lines carried *MYCN* in amplified versions in hsr regions and double minutes [16, 39, 40 (in press)]. Indications for both cytological forms of the amplicon in a single tumor cell were also found arguing for a transition between both manifestations [39]. Dmin are thus potentially persistent copies of the oncogene en route to integration at a host region on a different chromosome [41]. More recent findings, especially contributed by the cell line STA-NB10, promoted the episome model [40 (in press)]. Analyzing the borders of the *MYCN* amplicon by sequencing revealed a close match with the remaining ends on chromosome 2 after deletion. Furthermore, the two subclones of the cell line, STA-NB10/dmin and STANB/hsr, confirmed the hypothesis that integration of dmin at a different chromosomal location can form hsr with the same amplicon sequence.

The amplified region containing the *MYCN* gene can span DNA from 350kb to more than 1Mb with a consistent core region between 130 and 258kb including the gene itself [42, 43]. Additional DNA segments in proximal and distal orientation to the oncogene can be amplified to account for the rest of the size. Genetic analysis of the amplicon proved the coamplification of *DDX1*, *NAG*, *NSE1*, and *LPIN* on the telomeric side, and *EST-AA581763*, *SMC6* and *SDC1*

on the centromeric side with distance-dependant probabilities of coamplification (Figure 1) [44]. The effect of coamplification of neighboring genes in the *MYCN* amplicon on prognosis and disease outcome needs to be further elucidated. In case of *DDX1*, contradicting data has been published linking coamplification to faster relapse, on the one side, and beneficial prognosis and patient survival on the other [44, 45].

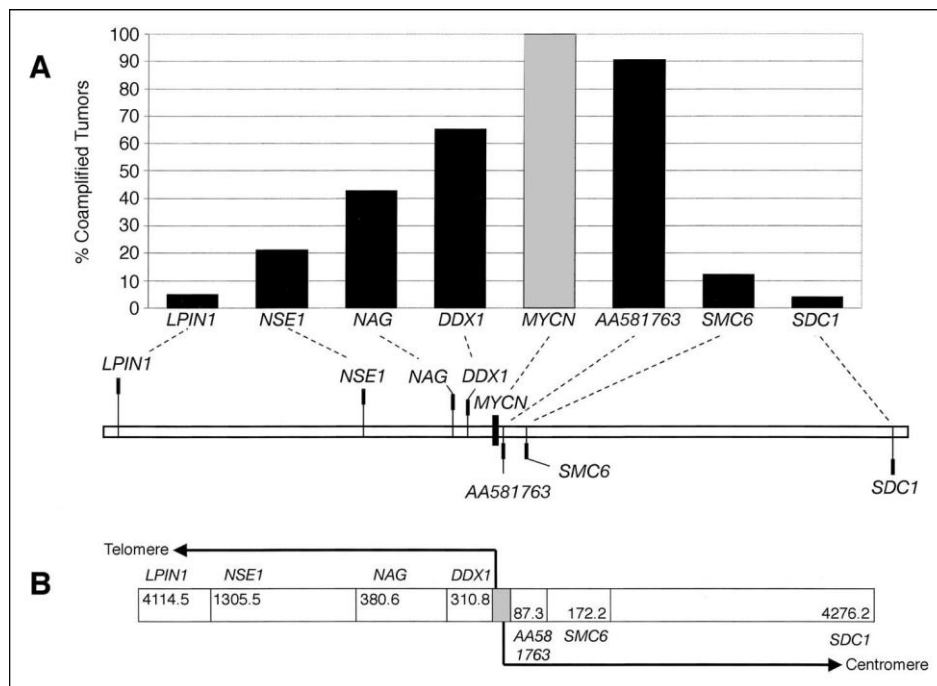


Figure 1: Coamplification in the *MYCN* amplicon is distance-related [44]. (A) Coamplification frequencies of the seven investigated genes on chromosome 2p24-25 in 98 primary NB tumors. **(B)** Physical distance of the seven investigated genes in relation to *MYCN*, based on current BLAT assignment information [42]

The *MYCN* gene in itself is generally not rearranged compared to its wild-type form and is usually amplified in a direct head-to tail tandem organization. A larger amplicon, however, undergoes internal rearrangements and deletions. During the course of the disease, the structure of the *MYCN* amplicon is considered to be invariable after the initial amplification process and found to be unchangeable in NB even by treatment [46]. Examination of the promoter region suggested that all copies of the gene can be transcriptionally active often resulting in the overexpression of the oncogene [47].

1.3 Intratumoral heterogeneity in neuroblastoma

By definition, heterogeneity in case of a disease refers to multiple etiologies of a medical condition. For instance, the cause of neuroblastoma is heterogenic in terms of different genomic alterations leading to the formation of a tumor in the extracranial nervous system. This kind of heterogeneity results in different stages and risk stratification of the tumor. *MYCN* amplification, loss of heterozygosity, gain of chromosome segments, whole chromosome aberrations, and ploidy in different combinations are characteristic for the aggressiveness of the tumor and relevant for its treatment. Additionally, patients were found with *MYCN*-amplified tumor cells in the bone marrow but showed no sign of amplification in the solid primary tumor, which is an example for heterogeneity in tumor cell populations in different locations of the body [48].

Intratumoral areas can also be genetically heterogeneous which was confirmed in multiple types of cancer. In some cases of renal cell carcinoma, heterogeneity in terms of DNA ploidy with different areas of diploid and aneuploid cells in the same tumor were detected [49]. Interphase FISH of meningiomas and flow cytometric analysis of small hepatocellular carcinoma evidenced a pattern of deviations in chromosome number among different cell clones [50, 51]. A study of human breast cancer, on the other hand, revealed heterogeneity concerning gene amplification within a tumor [52]. These are only a few examples of intratumoral heterogeneities, which relevant for the progression of the tumor and its treatment in some cases.

Although reported to a lesser extent, neuroblastomas also show heterogeneous areas in confined tumors. Kerbl *et al.* reported a case of a patient with a trisomic karyotype for chromosomes 1 and 2 in the majority of primary tumor cells [53]. In the same study, MNA or imbalances of 1p36 were also detected in different focal areas within the tumor. However, the first NB case with *MYCN* heterogeneity at the CCRI was already discovered in 1991. Heterogeneous tumors that were registered with the CCRI in the last decade were on average detected at a patient's age of 13 month. In contrast, patients with homogenous MNA tumors, that were included in the ANB94 study, were diagnosed with NB at an average age of 21 month (I.M. Ambros; personal communication). This difference argues for an earlier onset or faster growth to a detectable size of heterogeneous tumors. Metastatic growth, however, seems to be decreased since 55% of the tumors were assigned to localized and the 4S stage

(I.M. Ambros; personal communication). Whether this percentage is related to age and minor progression of the tumor or a veritable characteristic of heterogeneous tumors remains to be investigated in more detail. Interestingly, only 19% of the homogeneous MNA NB was classified as localized or 4S stages (I.M. Ambros; personal communication). Amplification of *MYCN* in a homogenous tumor cell population likely leads to a more rapid tumor progression and possibly contributes to metastatic growth. Cells of this more aggressive nature also seem to have the ability to overgrow neighboring tumor cells of more favorable genetics by faster, uncontrolled proliferation [54, 55]. A recent study with 20 NB patients was published with conflicting results on the involvement of single *MYCN*-amplified cells in heterogeneous tumors in relapse, progression, and dissemination [48]. Cases were found to argue for and against a lead role of these few cells. In the end, the authors reasoned that a small number of MNA cells in a tumor do not correlate with an adverse outcome.

In any case, the emergence of *MYCN* amplification resulting in heterogeneity of a localized NB tumor is only poorly understood and needs more focused investigation. For instance, it is not even known whether the heterogeneity in separate focal areas or diffuse cells originates from one or multiple tumor cell clones and whether these cells even carry the same amplicon.

1.4 Genetic instability in cancer

Genome instability is considered to be an important hallmark of cancer as reviewed by Negrini *et al* [56]. A number of cancers have revealed substantial chromosomal instability (CIN) often resulting in segmental or whole chromosome overrepresentation, aneuploidy or loss of heterozygosity (LOH). To a lesser extent, genomic instability was also found to involve the numeral reduction or expansion of oligonucleotide repeats present in microsatellite sequences (microsatellite instability or MIN) [57, 58]. Increased frequencies of base-pair mutations afforded by defective base excision repair have also been reported [59]. Point mutation instability (PIN) as manifested by an elevated rate of single nucleotide mutations is another form of instability and considered to be an important contributor to intratumoral heterogeneity [60]. An attempt to combine all these forms into one postulate of coherence and causality was done with the mutator phenotype hypothesis [61]. Under the

premise that normal DNA mutation rates are insufficient to account for the numerous mutations in a tumor, a mutator phenotype of cancer cells ensures the required frequency of genome-wide, irreparable DNA damage. However, a universal key event for the transformation of a normal cell to a tumor cell with mutator phenotype has not been identified thus far. More probable is the assumption that initiation of transformation has multiple, interchangeable origins with reciprocal influence on one another. For instance, an increase in genome-wide PIN can contribute to the development of CIN and MIN alike, especially when DNA repair genes are mutated at random [62-64]. Many hereditary cancers present genomic instabilities preceded by mutations in genes involved in DNA maintenance and integrity or DNA damage checkpoint - the so-called caretaker genes. Genes with inhibitory function on tumor growth or activator function in the apoptosis pathway are considered gatekeepers. Inherited germline mutations of either class of genes leaves a person with a higher predisposition for cancer [65]. A prominent example is the mutation of the two breast-cancer-susceptibility genes *BRCA1* and *BRCA2* leading to unresolved repair of DNA double-strand breaks and consequently to CIN [66]. Additional mutations of caretaker genes *ATM* and *TP53* certainly aid in the establishment of the mutator phenotype in breast cancer.

Mutation of caretaker or gatekeeper genes is a plausible explanation for genomic instability in inherited cancers. On the contrary, identifying similar somatic events which frequently underlie tumorigenesis of sporadic cancers has been met with difficulties and was largely unsuccessful [67-69]. A second model to explain genomic instability and the occurrence of CIN, characteristic for almost all sporadic cancers, is based on DNA DSBs induced by oncogenes. Activation of oncogenes and subsequently of the growth signaling pathway leads to DNA replication stress [70]. Sequences that are prone to break under this stress after inhibition of replication are termed "common fragile sites" [71-73]. The consequent, stress-related induction of LOH and genomic instability has been reported for mammalian cells in culture, mouse models and human xenografts [74-78]. For instance, within a single cell cycle, activated *ras* induces DNA DSBs in cultured NIH3T3 fibroblasts [76, 77]. Transcription factors MYC and E2F1, cell-cycle regulator Cyclin E, and the Mos protein kinase are expressed by other oncogenes which affect DNA integrity in a similar fashion [75, 76, 78, 79]. Interestingly, a number of these oncogenes were evidenced to play a more important role in the induction of apoptosis and/or senescence, the natural barriers to tumorigenesis, than in tumor progression. Upon formation of DNA DSBs, the DNA damage response (DDR)

pathway is normally activated culminating in P53 phosphorylation and the successional induction of cell cycle arrest, apoptosis, or senescence depending on severity of DNA damage and success of its repair [80]. Hereditary and sporadic cancers alike need to circumvent these responses in order to progress from a precancerous lesion to an advanced tumor [74]. For this reason, a strong selective pressure is placed on mutations in DNA checkpoint genes and especially on *p53*, which consequently the most widely mutated gene in human cancers [81].

1.5 DNA double strand break response and the histone H2AX

As previously stated, DNA double strand breaks are important initiators of genomic instability and involved in carcinogenesis [56]. Intracellular detection of DSBs leads to subsequent activation of the DSB response pathway. Members of the phosphoinositide 3-kinase (PI3K) - like family, namely the ataxia telangeictasia mutated (ATM), the ataxia telangeictasia and Rad3-related (ATR), and the DNA –dependent protein kinase (DNA-PK), are activated upon DSB formation and respond amongst other things by on-site phosphorylation of the downstream target H2AX at serine residue (Ser139) [82, 83]. Subsequently, phosphorylation of H2AX was shown to spread to molecules at increasing distance of the initial break site [84, 85]. This signal amplification cycle is induced by binding of the mediator of DNA damage checkpoint protein 1(MDC1) to γ H2AX and the recruitment of the Mre11-Rad50- Nbs1 (MRN) complex leading to further stimulation of ATM [86]. Chromatin modifications required for the recruitment of tumor suppressor p53-binding protein 1 (TP53BP1) is another implication of the feedback loop [87]. This association establishes a link between DNA DSB detection and tumor suppressor *p53*-mediated cellular responses. Different signaling pathways are activated when more proteins are recruited as a direct consequence of phosphorylated γ H2AX in order to converge to a successful repair of the DSB in the end. To name a few, MCPH1, a protein participating in sister chromatid condensation and cell cycle arrest, or other chromatin remodeling complexes involved in DNA repair accumulate at DSBs [88, 89]. ATR, induced by MCPH1, and ATM, phosphorylated by the γ H2AX-mediated feedback loop, relay activation to checkpoint kinases CHK1 and CHK2 [90-92]. This process is considered to prevent entry into mitosis. Defective

components of the DSB response pathway are tied in one way or the other to malignancies and other diseases which further illustrates the importance of an accurate DNA repair.

Ascertaining DSBs can be done by monitoring characteristics of certain members of the described response pathway. The intracellular localization of TP53BP1, phosphorylation status of Chk2, ATM and p53 or merely the p53 protein levels are commonly consulted as indicators for increased DNA DSB formation. Measuring γ H2AX, however, is advantageous to the aforementioned techniques. Due to the amplification of the phosphorylation, larger foci are detectable by specific antibodies to the phosphorylated serine residue. Since these foci form at the nascent sites of DSBs, counting of γ H2AX signals correlates well with the actual number of DSBs at least during the onset of repair [85, 93].

As a member of the H2A-family of histones, H2AX is contained on average in every fifth nucleosome in fibroblasts. The contingent in the histone H2A pool can however vary between cell types from 2% in lymphocytes to up 20% in human glioma cell lines [94]. The human H2AX gene (*H2AFX*), mapping to 11q23.2 to approximately 11q23.3 on chromosome 11, shows implications to genomic stability in certain cancers when the gene is targeted by mutations or deletion [95, 96]. In case of head and neck squamous cell carcinoma, loss of distal 11q including the *H2AFX* gene is frequently reported to associate with DNA repair deficiency [97]. A population-based genetic association study in non-Hodgkin lymphoma and a genetic screen of sporadic breast cancer revealed a direct effect of genetic variation and copy number alterations in the *H2AFX* gene on susceptibility to tumor development [98, 99]. All this data supports the notion that H2AX acts as a mediator of tumor suppression [100].

However, the direct affiliation of H2AX phosphorylation to genomic instability is not always feasible, since various factors account for DSB formation. In addition to a deficiency DNA repair of regularly occurring DSBs, direct interaction of DSB-inducing agents, reactive oxygen species (ROS), indirect interference of metabolites, eroded telomeres or viral infections originate DNA double strand damage [101]. Ionizing radiation (IR) and radiomimetic chemicals conduct a direct attack on DNA and exposure to these chemicals was thus linked to an increased risk of cancer development [84]. IR can also indirectly elicit DNA damage by interacting with cellular water to produce ROS, which can also be generated from endogenous metabolic sources, and were linked to carcinogenesis [102, 103]. ROS were shown to introduce DNA single strand breaks mostly during replication, which progress in an estimated 1% of the cases to double-stranded lesion [104]. The fact that metabolic processes

affect DNA integrity is exploited by numerous anticancer drugs, including cisplatin and hydroxyurea (HU), which interfere with the replication or transcription machinery resulting in DNA DSB formation. Hydroxyurea is an example for an alteration of the dNTP pool. HU inhibits the enzyme ribonucleotide reductase responsible for converting ribonucleotide triphosphate (NTPs) to deoxyribonucleotidetriphosphate (dNTPs) [105]. dNTPs are required in DNA replication. Other drugs, the camptothecins, inhibit cleavage of topoisomerase I (TOP1) by stabilizing its interaction with DNA and thus facilitate a potential collision with moving replication forks [106]. Such replication fork stalling often results in collapse and formation of DSB. The progression of topoisomerase II (TOPII) can also be compromised by binding of therapeutic agents like doxorubicin which stabilizes the TOPII-DNA complex after cleavage for tension release [107]. The DNA can thus not be resealed and DSBs are left behind. Attrition of telomeres in aging mammalian cells usually heads towards uncapped chromosomal ends when not maintained by telomerases. Since differentiated cells lack telomerases, unrepaired ends are detectable as DSBs by γ H2AX [108]. The cellular response to irreparable DSB can also lead to age-related senescence [109].

Due to its sensitivity, detection of γ H2AX is employed as a good tool for the assessment of cancer progression and therapeutic progress in clinic samples [101]. Additionally, organismal stress carried out by other environmental agents is increasingly determined by DNA damage induction and γ H2AX foci formation.

1.6 Neuroblastoma, genomic instability and DSB detection

Neuroblastoma is a sporadic cancer with only a few documented hereditary cases [15]. Genetic heterogeneity of this solid tumor is manifested by the variety of segmental and numeric genetic aberrations detectable in primary tumors and after relapse. Genomic instability leads to the most frequently observed alterations including allelic loss of chromosome 11q and a gain of 17q. Other aberrations involve 1p, 1q, 2p, 3p, 4p, 9p, and 14q to name a few [13]. Common mutations in caretaker or gatekeeper genes are not listed among the various genetic abnormalities of NB and major oncogenic pathways seem spared from deregulation in primary tumors. Reported gatekeeper abnormalities were only accounted for

in NB cell lines. In case of p53, cell lines established after cytotoxic treatment and relapse have frequently shown an increase in mutation in *p53* directly or other alterations affecting members of the p53/MDM2/ARF pathway [110, 111]. *Ras* is another oncogene which is often targeted by activating mutations and was shown together with mutated p53 and APC to be responsible for chromosomal aberrations in colorectal adenocarcinomas [112]. Although *Ras* can block *MYCN* degradation and thus promotes cell cycle progression in cultured LAN-1 cells [113], an activating mutation of the oncogene has thus far not been detected in primary neuroblastoma, not even at advanced stages with *MYCN* amplification. The increase in copy number of *MYCN* is the only prevalent alteration of an oncogene in NB observed in around 20% of primary tumors [114].

The fact that only roughly a fourth of all neuroblastoma cases show a *MYCN* amplification permits the assumption that these tumors potentially carry one or a constellation of genetic factors predisposing for MNA, which non-amplified tumors do not. While two prominent hypotheses with the breakage-fusion-bridge cycle and the episome model have been established illustrating the actual mechanism of gene amplification [32-37], a universal trigger for this event and *MYCN* amplification in particular has not been found yet. For this reason, we focused on the examination of the genomic background in neuroblastoma looking for a common genomic aberration that might predispose for MNA. Since “classic”, homogeneous MNA tumors are already advanced in development, we chose to investigate the genetic profile of NB with heterogeneous MNA. The advantage of heterogeneous tumors lies in genomic data contributed by surrounding tumor cells without MNA. These cells might either still develop amplification themselves or play an independent role in triggering MNA formation in other tumor cells. Both genomic instability and the initial step of amplicon manifestation are closely tied to DSB formation. Therefore, our second, major focus was the investigation of DSB occurrence by γ H2AX detection and subsequent correlation to the *MYCN* copy number in order to shed light on overall DNA integrity in *MYCN*-amplified cells. We also tested the suitability and accuracy of the standard NB diagnosis protocol set up by the INRG Biology Committee applied to detection of MNA heterogeneity and amplicon composition in neuroblastoma [115].

2 Patients, Materials and Methods

2.1 Patients

A total of thirteen tumor pieces of five neuroblastoma patients was analyzed in this study. Clinical and therapy data is summarized in Table 1. Staging was done in accordance with the International Neuroblastoma Staging System. All thirteen tumor pieces were collected from the tumor library of the Children’s Cancer Research Institute (CCRI, Vienna, Austria) and selected for their reported genetic heterogeneity in *MYCN* amplification. Reference samples of homogeneous tumors were grouped according to their MLPA profile and also taken from the CCRI tumor library.

Patient #	Stage	Age at diagnosis	Localization	Therapy	Outcome	Number of tumor pieces
1	3	3.5 years	left-hand side part of abdominal cavity, infiltrating across the midline, kidney, spleen	HR-NBL; autoSCT; radiotherapy; Roaccutane	death	1
2	2A	11 months	thoracic-abdominal	INES CHT	CR	4
3	3	10 months	adrenal right	NB94	CR	2
4	2B/4/4S	11 months	thoracic left	INES NB99.4	CR	4
5	3	9 months	adrenal right	NB94	CR	2

Table 1: Clinical and therapy data of the five patients selected for genetic analysis.

2.2 Microscopic techniques

2.2.1 Preparation of frozen patient material

Patient tumor samples were embedded in Tissue Freezing Medium (Jung, Nussloch, Germany; Cat. No. 020108926) on metal specimen disks and cut at 5µm with Leica low-profile disposable blades type 819 in a Leica CM1850 UV. Sections were picked on Premium HistoFrost Plus microscopic slides (Stölzle-Oberglas GmbH, Vienna, Austria; Prod. No.: 04-2009) and stored at -20°C until further use.

2.2.2 Histochemistry of frozen sections

For histochemical analysis of the tumor samples, sections were stained with hematoxylin and eosin. Slides were placed in deionized water for 2 minutes to wash of the mounting medium before incubation in hematoxylin (Mayer's hemalum solution for microscopy, filtered, Merck, Cat. No. 1.09249.0500) for 8 minutes. The blue color of the nucleus was then developed under running tap water, a process called blueing, for 30 minutes before treating the sections with eosin for up to 30 minutes depending on the age of the eosin (Eosin Y (Yellowish), Merck, Cat. No. 15935). Afterwards, the sections were dehydrated in an ethanol series (70% EtOH for 10sec, 96% EtOH for 2min, and 100% EtOH for 2min) before placing the slides into xylene for 10min. Then, slides were air-dried, embedded in Entellan rapid mounting medium for microscopy (Merck, Darmstadt, Germany; Cat. No. 1.07960) and covered with cover slips. Inspection of the tumor samples for sample quality, and tumor cell and stroma content was done with a Leica Axioplan 2 microscope in the transmitted light mode.

2.2.3 DNA probe labeling by nick translation for FISH

The bacterial clones RP11-355-H-10 (AC010145, *MYCN*), 08-103-1 (chromosome2p), RP11-422-A-6 (*DDXI*) and RP11-685-A-8 (*NAG*) were obtained from Dr. M. Rocchi (Resources for Molecular Cytogenetics, University of Bari, Italy). 2µg of the respective DNA were combined with either DIG-Nick Translation Mix (Roche, Vienna, Austria; Cat. No. 11745816910) containing 0.08 mM digoxigenin-11-dUTP or Biotin-Nick Translation Mix (Roche, Vienna, Austria; Cat. No. 11745824910) containing 0.08 mM biotin-16-dUTP respectively and the total volume adjusted to 40µl with ddH₂O. The *MYCN* probe was labeled with DIG and the others with biotin. The solutions were incubated for 90minutes in a water bath at 16°C. To verify complete digestion and size (*MYCN*: 200 Kb) of the probes after the very first digestion, 5µl of the respective probe sample was run with 1µl loading buffer in a 1.2% agarose gel at 100V and 500mA. Meanwhile the probes were kept on ice so that further nick labeling remained possible. The reaction was stopped by addition of 30µg of COT human DNA (Roche Diagnostics GmbH, Mannheim, Germany; Cat. No. 11581074001), a volume of NaAc (3M, pH 5.5, Merck, Darmstadt, Germany; Cat. No. TA636468) calculated as 1/10 of the probe volume plus the Cot- DNA volume and 2.5 times the volume of the solution of ice cold 100%EtOH (Merck, Darmstadt, Germany). Precipitation of labeled DNA probes was achieved by incubation at -80°C for a minimum of 30 minutes. The following centrifugation was done for 30 minutes at 13000 rpm at 4°C with a Hereaus Biofuge pico. After discarding the supernatant, the pellet was resuspended in 70% EtOH (local Pharmacy, Vienna) followed by centrifugation for 15 minutes at 13000rpm at 4°C. The supernatant was again removed and the DNA pellet dried for 5 minutes at RT. Resuspension of the probe was done in 40µl of a master mix and the DNA dissolved at 37°C in an Eppendorf thermomixer compact. The probe mixes were stored at 4°C until further usage.

2.2.4 Two-color interphase fluorescent in situ hybridization

Cryosectioned slides were placed into 1xPBS for 5 minutes prior to fixation with 4% paraformaldehyde (Roti-Histofix 4%, Roth, Karlsruhe, Germany; Cat.No. P087.3) for 12 to 14 minutes at 4° C. Sections were then either permeabilized with 0.1% Triton X100 in 1xPBS for 5min at RT or permeabilized with 0.5% Triton X100 in 1xPBS for 5min at RT, washed twice with 2xSSC for 5minutes before and after incubation with 100µl of 0.1mg/ml RNase (Sigma-Aldrich, Germany; Cat. No. R-5000). After permeabilization with or without RNA digestion, the sections were treated with a 0.005 µg/µl pepsin-containing solution for protein digestion. Incubation time depended on the exposition of cells to the enzyme. The progress of digestion was controlled under a Zeiss Axioplan 2 microscope in the transmitted light mode. If cells needed more digestion, the slides were placed into the Pepsin solution again. General incubation times varied between ½ and 1 minute. After digestion, the slides were washed twice with 1xPBS for 5 minutes at RT before dehydration in an ethanol series (70%, 96%, 100% EtOH for 2 minutes each) and air-drying of the sections. Depending on the area of the section, 1µl to 2µl of each respective nick-labeled probe were applied to the section. Slides were then covered with a coverslip and sealed with rubber cement (Fixogum, Marabu, Tamm, Germany; Cat. No. 290110000). Denaturation of probe and target DNA was performed on a hot plate (Präzitherm, Störcktronic) at 78°C for 8 minutes. The slides were incubated for hybridization over-night or over the weekend in a moist chamber in a Haereus incubator at 37°C. Following incubation, the slides were washed for 5 min in 2 x SSC at RT. For stabilization of the DNA::probe duplex, the sections were incubated for 15 min in 50% formamide in 2 x SSC and rinsed twice with 2 x SSC both at 42°C. The labeled probes were then detected with the respective antibody either against digoxigenin or biotin in a dilution with 2% bovine serum albumin (BSA) (Sigma-Aldrich)/1xPBS. A volume of 100µl of a mixture of a mouse Cy3-conjugated IgG Anti biotin (Jackson Immuno Research Laboratories, Cat. No. 200-162-096) diluted 1:500 and sheep anti-digoxigenin FITC-conjugated antibody (Enzo Life Sciences, Inc., Farmingdale, NY, USA; Cat. No. 12077441) diluted 1:100 was used for probe detection. Incubation was performed in a moist chamber at 37° C for 30 to 45 min followed by washing twice for 7 minutes in 4 x SSC/ 0.1% Tween 20 at 42° C. Secondary antibodies diluted in 2% BSA/1xPBS, were incubated in a moist chamber at 37°C for 30 minutes followed again by the washing procedure described above. Fixation of the

staining was achieved by incubation of the slides in 4% paraformaldehyde in 1x PBS for 20 minutes at 4° C, followed by washing twice for 5 minutes in 1x PBS, dehydration in EtOH as above and air drying in the dark. Slides were mounted with Vectashield (Vector, Burlingame, Ca, USA; Cat. No. V0305) supplemented with DAPI, covered with a cover slip, and sealed with rubber cement. Slides were photographed with an Axioplan2 fluorescence microscope (Zeiss, Austria) and images analyzed with the ISIS V 5.2.20 software by MetaSystems (Altlusheim, Germany).

2.2.5 γ H2AX immunohistochemistry on cryosections

For the detection of DNA double strand breaks on a cellular basis, cryosections of tumor samples were stained for the histone variant γ H2AX and subsequently hybridized with *MYCN* FISH probe. Cryosections were either air dried at room temperature following sectioning or thawed after storage at -20°C. After a washing step with 1xPBS at RT for 5 minutes for the removal of the Tissue Freezing Medium, the sections were fixed in methanol/acetone (1:1) at -20°C and washed again with 1xPBS for 5 minutes. The slides were then fixed for 15 minutes at RT with 4% paraformaldehyde (Roti-Histofix 4%, Roth, Karlsruhe, Germany; Cat.No. P087.3) before washing three times with 1xPBS for 5 minutes each at RT. Afterwards, the sections were permeabilized with 0,1% TritonX100, 0.1% SDS in 1xPBS for 6 minutes at RT. The tissue was blocked with a blocking solution of 5% goat serum (normal) (Dako, Denmark; Code X0907), 1% BSA in 1xPBS. The anti-phospho-histone H2A.X (Ser139), clone JBW301 antibody from Millipore, Vienna, Austria (Cat. No. 16-202A) was diluted 1:500 with a solution of 1% goat serum (normal), 1% BSA in 1xPBS. The sections were incubated with the antibody solution for 60 minutes in an incubator at 37°C. The slides were washed three times while slowly shaking with 1xPBS for 5 minutes at RT. The Cy3-labeled goat-anti-mouse secondary antibody was applied at a 1:500 dilution with 2% filtered BSA for 45 minutes in a 37°C incubator. After two additional washing steps, the slides were counterstained with a 2 μ l/ml DAPI (Sigma-Aldrich, Germany; Cat. No. D9542) in 1xPBS solution for 1 minute at RT. The DAPI solution was removed by washing while gently shaking with 1xPBS for 10 minutes at RT. The sections were then covered with Vectashield (Vector, Burlingame, Ca, USA; Cat. No. V0305) and a cover slip and sealed with rubber cement.

Single images were taken with the Metafer 4 software by MetaSystems (Altussheim, Germany) on a Zeiss Axioplan2 fluorescence microscope (Zeiss, Austria) run in an automatic mode at a 40-fold magnification. The integrations time for the detection of Cy3-labeled γ H2AX and DAPI was fixed. The single images were stitched to an overview of the entire section with the MetaSystems Virtual Slide software.

2.2.6 MYCN I-FISH on γ H2AX- prestained tumor sections

To correlate the occurrence of DSBs with *MYCN* amplification in neuroblastoma, *MYCN* I-FISH was performed on γ H2AX- prestained tumor sections. Coverslips were removed and the slides washed twice in 1xPBS for 5 minutes at RT. Sections were then permeabilized with 0.5% TritonX100 in 1xPBS for 5 minutes at RT before washing the slides twice with 2xSSC for 5 minutes each. RNA was digested with 0.1mg/ml RNase (Sigma-Aldrich, Germany; Cat. No. R-5000) at 37°C for 60 minutes before washing the sections twice again with 2xSSC. Slides were then incubated for 30 seconds in a pepsin-containing solution and washed twice with 1xPBS for 5 minutes each at RT. Afterwards, the sections were dehydrated in an ethanol series (70%, 96%, 100% EtOH for 2 minutes each) and air dried. 3 μ l of the DIG-labeled *MYCN* FISH probe were applied to a section. The rest of the procedure largely followed the instructions described in 2.2.5. For detection of the DIG-labeled *MYCN* probe, a sheep anti-digoxigenin, FITC-conjugated antibody (Enzo Life Sciences, Inc., Farmingdale, NY, USA; Cat. No. 12077441) was diluted 1:100 in 2%BSA and applied for 45 minutes at 37°C.

Single images were taken automatically with a position list of the field-of-vision (FOV; (MetaSystems)) coordinates of the corresponding γ H2AX-stained sections and section overviews were obtained as described in 2.2.5. The integrations time for the detection of FITC-marked *MYCN* was fixed. Correlation of single γ H2AX- and *MYCN*-FISH-stained images was done manually with imageJ 1.40g (National Institutes of Health, USA).

2.3 Genomic evaluations of tumor samples

2.3.1 DNA extraction from tumor samples

For DNA extraction, the tumor was cut into smaller pieces and put into a pp-tube. The sample was then washed and spun down with an erythrocyte lysis buffer at 500g (~1700rpm) for 5 minutes with a Heraeus multifuge 1S-R centrifuge (Thermo Scientific). The supernatant was discarded and 3ml lysis buffer, 25µl Proteinase K (20mg/ml) (Sigma-Aldrich, Germany; Cat. No. P-6556), and 125µl SDS (20%) added in this order to the pellet. The sample was incubated at 56°C over night. After the overnight incubation, 1ml 6M NaCl was added to the lysis buffer- mix and centrifuged at 3450g for 30 minutes. The supernatant was then transferred to a new tube and the DNA precipitated with 2x vol. of 100% EtOH. Afterwards, 50µl 1x TE buffer was filled into an Eppendorf tube in advance, before transferring the DNA precipitate. The DNA was stored at 4°C until further use.

2.3.2 Multiplex ligation-dependent probe amplification (MLPA)

MLPA is a variation of the standard polymerase chain reaction (PCR) reaction and permits multiple DNA targets to be amplified by a single primer pair ligated to different probes. The DNA sample was diluted to around 100ng/5µl end concentration with 1x TE-buffer in a 0,5ml PCR tube. The MLPA procedure requires 15µl of the DNA dilution. For each DNA sample, 5µl were pipetted into three different 0,5ml PCR tubes. The tubes were placed into a T3000 thermocycler from Biometra and the DNA was denatured at 96°C for 5 minutes and cooled again to 25°C. Afterwards, 3µl of the three different hybridization mixes were added (see Table 1 for all reaction mixes). Each mix contained the respective Salsa Probe mix for the detection of NB - P251, P252, and P253 – and was applied to only one of the three PCR tubes. The samples were first heated to 95°C for 1 minute and then the probes hybridized at 60°C for at least 16 hours. Next, the samples were cooled to 54°C before applying 32µl of the Ligase-65 mix per tube. The ligation was then run for 15 minutes at 54°C before the ligase was inactivated and the DNA was denatured at 98°C for 1 minute. The samples were then kept at 10°C until further processing. In the meantime, fresh PCR tubes were prepared with

15µl of the PCR mix each. After the ligation program was finished, 5µl of the ligation reaction was transferred into the new PCR tubes. The PCR tubes were then put into the thermocycler and heated to 60°C before adding 5µl of the polymerase mix to each tube. The ligated probes were then amplified in 35 cycles of denaturing at 95°C for 30 seconds, annealing at 60°C for 30 seconds and elongation at 72°C for a minute. A final elongation step was afterwards performed at 72°C for 20 minutes before the program was put on hold at 10°C. The samples were stored at 4°C until the next processing step. Separation of the amplified PCR products was done with capillary electrophoresis. A MicroAmp plate (Applied Biosystems, Darmstadt, Germany; Cat. No. N801-0560) was filled with 9.3µl of the electrophoresis mix per needed well and 1µl of the PCR product added before the wells were sealed. The samples were then analyzed with an ABI prism 3100 (Applied Biosystems). The data readout was interpreted with the MLPA Vizard software from the Austrian Research Center GmbH (Vienna, Austria).

Name of Mix	Component	1 reaction (µl)
Hybridisation Mix	Salsa Probe Mix	1.5
	MLPA Buffer	1.5
Ligase-65 Mix	Ligase-65 Buffer A	3
	Ligase-65 Buffer B	3
	Aqua dest.	25
	Ligase-65	1
PCR Mix	10x Salsa PCR Buffer	2
	Aqua dest.	13
Polymerase Mix	Salsa PCR-primers	1
	Enzyme Dilution Buffer	1
	Aqua dest.	2.75
	Salsa Polymerase	0.25
Electrophorese Mix	Standard 500 Rox	0.3
	HiDi formamide	9

Table 2: MLPA reaction mixes. Depending on the number of DNA samples the reaction mixes were done as master mixes. All reagents were obtained from MRC Holland except for aqua dest. and HiDi-formamide (Applied Biosystems, Darmstadt, Germany; Cat. No. P/N4311320C).

2.3.3 Single nucleotide polymorphism (SNP) array

The Affymetrix GeneChip® Mapping 500K Assay was used in conjunction with the GeneChip® Mapping 500K set for the investigation of copy number alterations and segmental aberrations in the genome of hetMNA neuroblastoma. The protocol on the Affymetrix, Inc. (Santa Clara, CA, USA) support homepage ([https://www.affymetrix.com/support/downloads/manuals/500k assay manual.pdf](https://www.affymetrix.com/support/downloads/manuals/500k_assay_manual.pdf)) was largely followed as instructed and reagents listed for the low throughput protocol were used. In short, approximately 250ng total genomic DNA was taken for each SNP array. The tumor DNA was digested with the restriction enzyme NspI before ligating the fragments to adaptors with a T4 DNA ligase. The ligation products were then amplified by PCR with generic primers recognizing the adaptor sequence. After purification of the PCR products, the amplified DNA was fragmented by DNaseI and labeled with biotin. The labeled DNA probes were hybridized to the NspI GeneChip® Mapping 250k array of the 500K array set. After hybridization, excess probes were washed from the arrays in an Affymetrix Fluidics Station 450 and hybridized probes marked with streptavidin-phycoerythrin. The arrays were scanned using a confocal laser GeneChip Scanner 3000 (Affymetrix, Inc., Santa Clara, CA). In total, thirteen hetMNA NB tumor pieces from 5 patients were analyzed with the NspI 250K array.

Data analysis was performed using the CNAG (Copy Number Analyzer for Affymetrix GeneChip Mapping arrays) software, version 3.0 (GenomeLaboratory, Tokyo University, <http://www.genome.umin.jp>) [116, 117]. The UCSC genome browser, assembly May 2004 (<http://genome.ucsc.edu/>) was used to annotate and visualize regions of segmental chromosomal aberrations, gene amplifications and deletions.

2.4 Buffers and Solution

1xPBS

47,75g	PBS powder (Applichem, Darmstadt, Germany; Cat. No. A0964.9050)
5l	deionized H ₂ O

Eosin solution

For 100ml working solution a 1:10 dilution of Eosin stock solution with deionized H₂O as done with the addition of:

5gtt 96% acetic acid (Merck, Darmstadt, Germany; Cat. No. 1.00062.2511)

5gtt 37% Formaldehyde (Merck, Darmstadt, Germany; Cat. No. 1.04003.1000)

3M Na-Ac

2,46g	Na-Acetate (Merck, Darmstadt, Germany; Cat. No. TA636468)
10ml	dH ₂ O

Master mix for nick translation

500µl	Formamide (Merck, Darmstadt, Germany; Cat. No. 1.04003.1000)
100µl	20x SCC (Applichem, Cat. No. A4506.5000)
200µl	Dextran sulfate
200µl	dH ₂ O

Pepsin-containing solution

0.5ml	HCl
49.5ml	deionized H ₂ O
25µl	100mg/ml Pepsin (Sigma-Aldrich, Germany; Cat. No. P- 7012)

Erythrocyte- lysis buffer

4,15g	NH ₄ Cl
0,5g	10mM KHCO ₃
100µl	0,5M EDTA pH8.0 (Gibco, Auckland, New Zealand; Cat.No. P1513)
500ml	deionized H ₂ O

Lysis buffer

1,21g	Tris pH8.0
23,376g	NaCl
0,744g	EDTA

TE buffer

5ml	1M Tris pH7.6 or pH8.0
1ml	0,5M EDTA
494ml	deionized H ₂ O

3 Results

3.1 Detecting *MYCN*- heterogeneity in neuroblastoma

3.1.1 Hematoxylin and Eosin stainings help in estimating tumor cell content but FISH is needed for detecting tumor heterogeneity

In order to investigate the applicability of the histology-based, diagnostic workup of a heterogeneous NB tumor, we compared HE stainings to *MYCN* I-FISH-based detection of heterogeneity. Amplified tumor cells are generally identified by their *MYCN*- copy number with the respective FISH-probe according to the international consensus for neuroblastoma molecular diagnostics [115]. For the tumor to be categorized as “intratumoral heterogeneous”, surrounding non amplified cells also need to be identified as tumor cells which can be done by looking at the aneusomy of their chromosomes with specific FISH probes. In case of *MYCN*- amplified tumors, a probe to the centromere or the long arm of chromosome 2 is used as reference. HE stainings fail to show a clear difference in the morphology of *MYCN*- amplified and unamplified tumor cells within heterogeneous tumors and can thus not be used to identify heterogeneous tumors. On the other hand, information on the overall tissue morphology obtained by HE staining can be helpful for future tissue processing such as FISH stainings or microdissections. Figure 2A shows a picture of an area of a tissue section where tumor cells appeared well separated from one another and were thus accessible to the numerous reagents used during FISH staining. The area depicted in Figure 2B shows more fibrous stroma (Eosin pink) with embedded cells. These cells were generally less accessible for probe hybridization and needed a longer permeabilization or digestion in the FISH protocol. A longer digestion time, however, often led to the morphological destruction of more exposed nuclei. Stroma also showed a strong fluorescent background especially in the FITC- channel.

Figure 2C features an *in situ* hybridization of FITC-labeled *MYCN* and Cy3-labeled D2Z probes. Disomic cells of unknown type (white arrows), which were potentially tumorigenic, and trisomic tumor cells (red arrow) were detected in the merged image with DAPI in the upper panel. A different staining with another NB marker is needed in addition to unequivocally identify the disomic cells as tumor cell. The lower panel features the same

staining of a different area with *MYCN* amplified (red arrow head) and non-amplified (red arrow) cells. In certain cases of NB, aneusomies and *MYCN* amplification can thus be detected with this combination of probes for chromosome 2. Since most NB are aneusomic for at least one chromosome, tumor cells can be easily differentiated from normal cells or from one another in case of heterogeneous tumors with the appropriate set of probes.

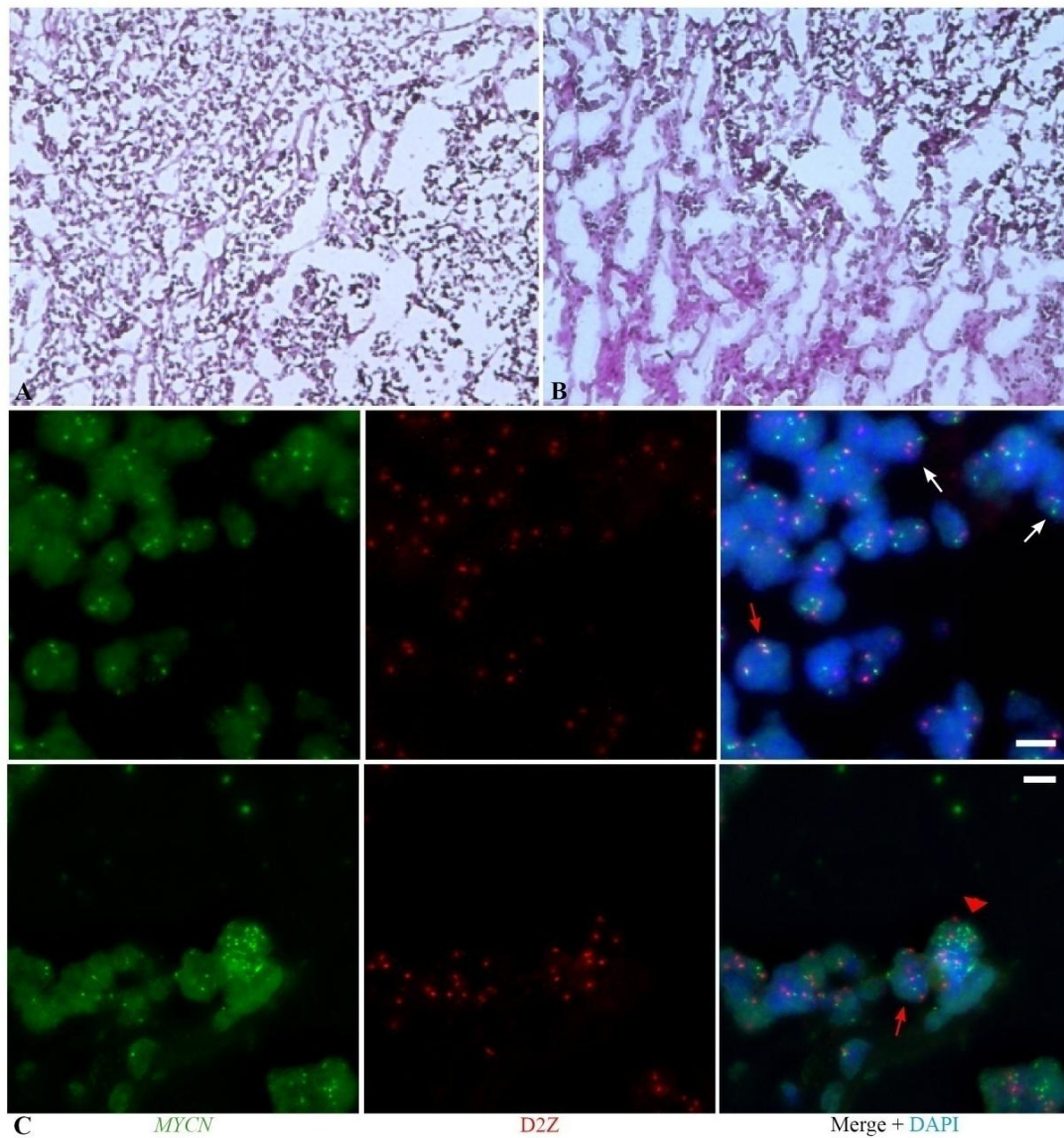


Figure 2: Histopathological and interphase FISH stainings of tumor sections. All sections were cut at 5µm in a cryostat. **(A)** Histopathological HE staining of fibrous stroma-poor area of a NB section. **(B)** HE staining of a stroma-rich area of a tumor section. **(C)** FITC-, Cy3- and merged image with DAPI background of an area in a heterogeneous NB section. *MYCN* is green, D2Z red and DNA blue. White arrows mark disomic cells, red arrows mark tumor cell trisomic for chromosome 2 and the red arrow head a *MYCN* amplified cell. White bars, 10µm.

3.1.2 Comparison of two-color *MYCN* I-FISH, MLPA and SNP array analysis for the detection of *MYCN* heterogeneity in neuroblastoma

The international consensus for neuroblastoma molecular diagnostics set up by the INRG biology committee requests I-FISH for the unambiguous diagnosis of *MYCN* amplification in NB [115]. Furthermore, pan-genomic, DNA-based investigations, like MLPA, array CGH or SNP array analysis are commonly conducted to determine genetic aberrations and can usually also show *MYCN* amplification [118]. In this experiment, DNA and the corresponding tumor piece were used to compare *MYCN* I-FISH, MLPA and SNP array analysis in terms of sensitivity and accuracy in the detection of *MYCN*-amplified cells and genes comprised in the amplicon.

For the mere detection of *MYCN* amplification by I-FISH, the *MYCN* probe was complemented by a reference probe for the centromeric region of chromosome 2 (D2Z) to illustrate the underlying chromosome copy number. A combination of probes to *MYCN* and adjacent genes *NAG* or *DDXI* was applied to give a more detailed profile of the *MYCN* locus and to confirm potentially coamplified genes. In case of coamplification of a gene in the *MYCN* amplicon, the signal of its probe was expected to equal the number of *MYCN* signals in a cell. Fluorochromes FITC (green) and TRITC (red) were used to immunofluorescently label *MYCN* and the reference probe, respectively, for fluorescence microscopy. Colocalization resulted in a yellow spot. Cells without MNA were expected to display the same number of colocalizations as the copy number of chromosome 2. In contrast to single-cell detection with I-FISH, MLPA and SNP arrays are based on genomic DNA and designed to give an average copy number of sequence in the extracted tumoral DNA. Since multiple probes were simultaneously hybridized to cover a chromosome, aberrations of any kind were detectable on a larger genome basis. The MLPA kit employed in this experiment was custom-designed with probes targeting a few preselected chromosomes of importance in NB detection. The 250k SNP array covered all chromosomes except the Y-chromosome with probes hybridizing to 250000 scattered single-nucleotide polymorphisms in the genome. SNPs were also used to investigate chromosomal copy numbers and genetic aberrations in the background of hetMNA tumors.

The MLPA diagram in Figure 3A shows a clear amplification of the *MYCN* oncogene (red rectangle). The size of the amplicon was rather small and neither *DDXI* nor *NAG* appeared

coamplified. The rest of the probes targeting chromosome 2 were rather uneven with a few outliers. Nonetheless, there was a good chance for an overrepresentation of the entire chromosome underlying MNA. The SNP array data in Figure 3B confirmed both *MYCN* amplification and the overrepresentation of chromosome 2. *MYCN* I-FISH data on this tumor corresponded well with MLPA and SNP array results. Although the nuclei contours were not always clearly separable, *MYCN* staining (green) and its reference signal from the centromeric D2Z probe (red) (Figure 3C) showed a clear imbalance in many cells. White arrows mark *MYCN* amplified cells in the figures. According to the INRG biology committee's criteria [115], a large number of NB cells classified as *MYCN*-amplified. The copy number of the *MYCN* gene was more than fourfold in comparison to the centromeric reference probe. The assumption that *DDXI* was not coamplified was verified by FISH results using *MYCN* and *DDXI* probes in a two color FISH experiment (Figure 3D).

However, the limitation of MLPA to detect rare amplified cells is shown with the tumor sample of Figure 4. The MLPA data showed a rather uniform overrepresentation of the entire chromosome 2, while an amplification of *MYCN* and genes surrounding the *MYCN* locus was not detected (Figure 4A). SNP arrays were also incapable of detecting a *MYCN* amplification but affirmed the overrepresentation of chromosome 2 (Figure 4B). On the contrary, I-FISH identified a number of tumor cells with increased copies of *MYCN* in comparison to the D2Z reference. Despite the fact that the contours of single nuclei were not always easy to determine, the number of *MYCN* signals clearly surpassed the two to three copies suggested by MLPA for the entire chromosome. White arrows mark amplified cells in the merged image of Figure 4C. Not only was the detection of rare cells carrying *MYCN* amplification unsuccessful by MLPA and SNP array but consequently the coamplification of *NAG* was missed as well (Figure 4D).

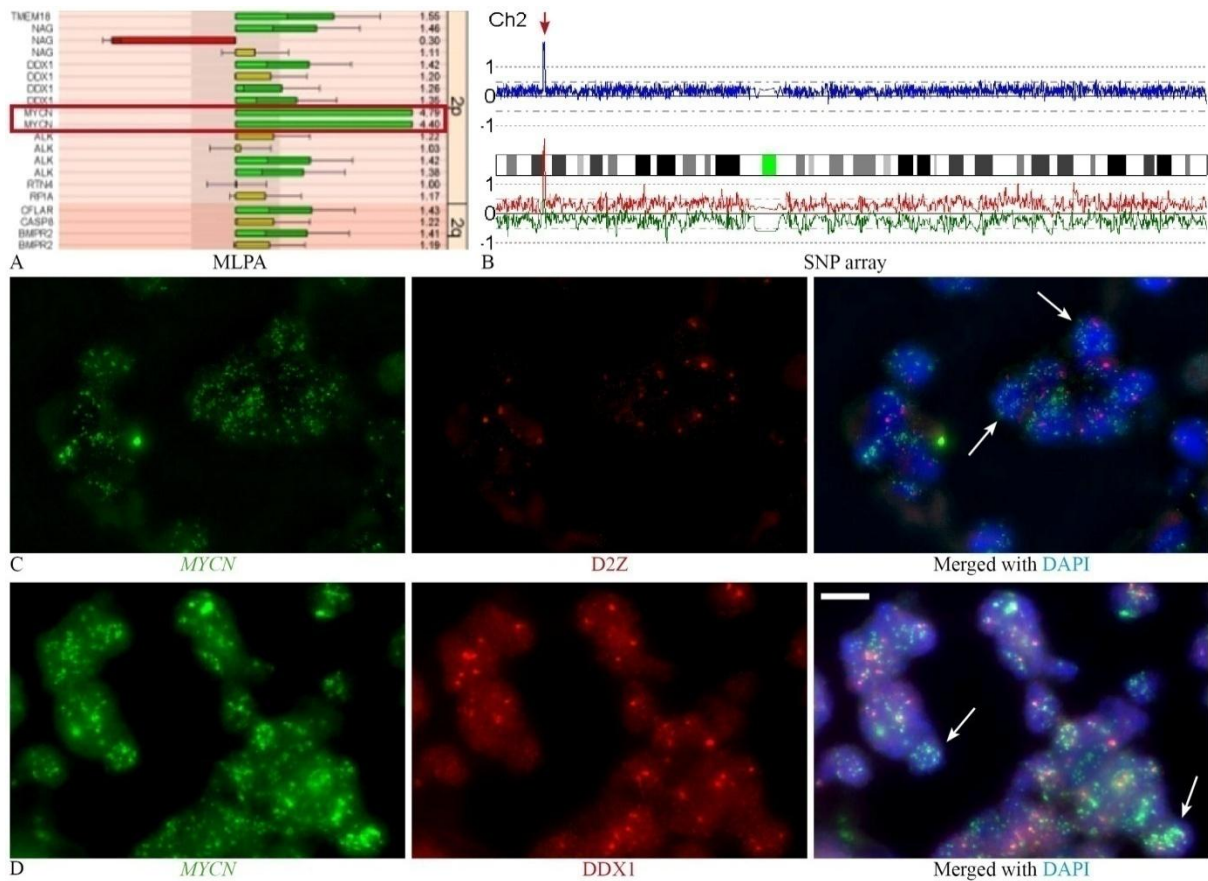


Figure 3: Comparison of MLPA and FISH results on *MYCN* amplicon detection and composition. Examination of a tumor DNA from patient #4 is done by MLPA (A) and SNP array analysis (B). The red rectangle in the MLPA readout of chromosome 2 marks the two *MYCN* probes. In the SNP array data, *MYCN* amplification is marked by the red arrow in the single-chromosome view of chromosome 2. The blue line illustrates the average copy number of both alleles; red (large) and green (small) lines depict allele based analyses. Chromosomes are represented by their cytoband information. Interphase fluorescent *in situ* hybridization (FISH) validates of MNA with *MYCN* (green) and D2Z (red) probes (C). Composition of the *MYCN* amplicon is confirmed with probes for *MYCN* (green) and *DDX1* (red) (D). White arrows point out good examples of *MYCN*-amplified cells. White bar, 10 μ m.

Due to the nature of the tissue, contours of single nuclei are again rather diffuse in large areas of the section. However, the density of characteristic yellow signals for colocalization of FITC- and Cy3-labeled FISH probes in areas of approximately the regular size of a nucleus were taken as a clear indication for coamplification of *MYCN* and *NAG* in this tumor sample. Non-*MYCN*-amplified nuclei also showed close proximity of probes for *MYCN* and *NAG* but only the two to three signals per nucleus which were expected from the MLPA and SNP array results.

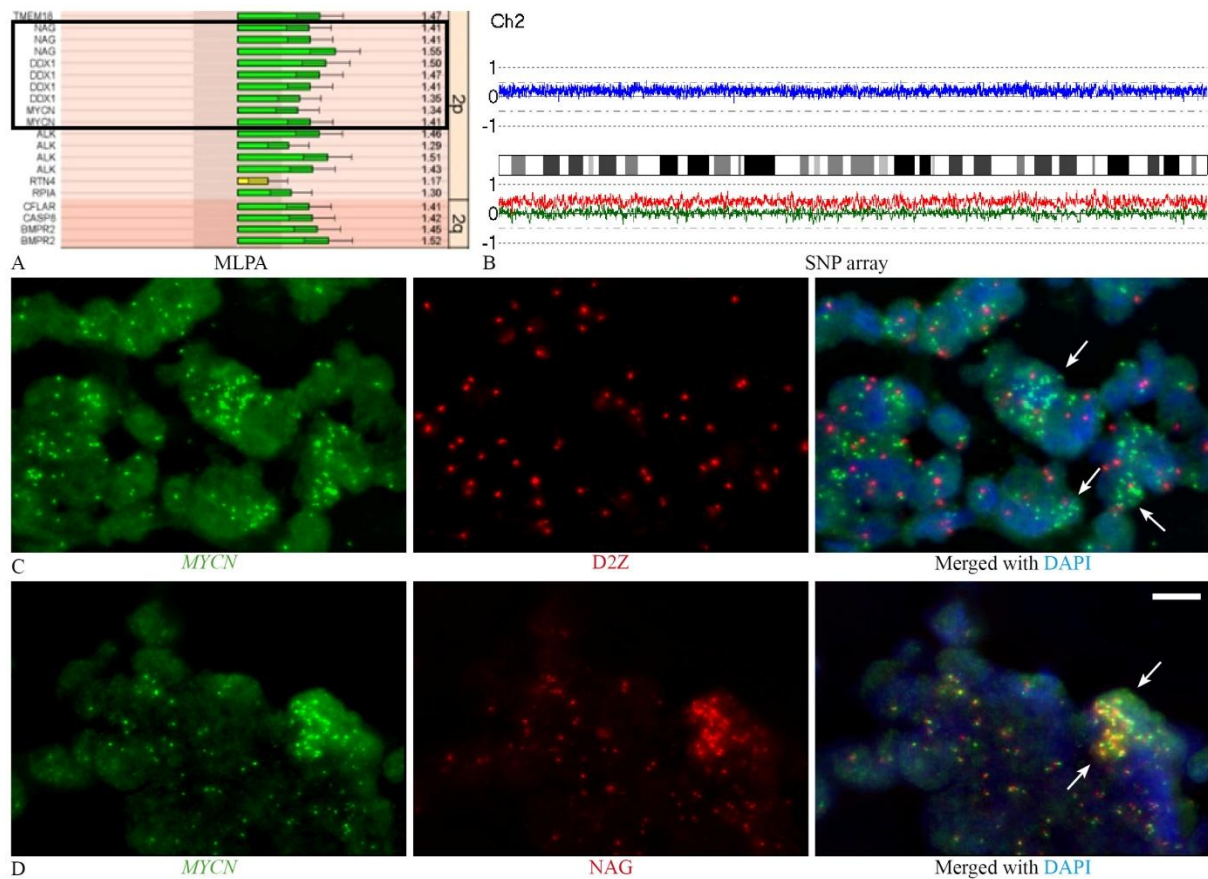


Figure 4: MLPA and SNP array of a heterogeneous tumor do not always correlate with *MYCN* I-FISH results. Examination of a patient's tumor DNA is done by MLPA (A) and SNP array analysis (B). The black rectangle in the MLPA readout of chromosome 2 frames the probes often comprised in a *MYCN* amplicon. The SNP array data is displayed in the single-chromosome view of chromosome 2. The blue line illustrates the average copy number of both alleles; red (large) and green (small) lines depict allele based analyses. Chromosomes are represented by their cytoband information. Interphase fluorescent *in situ* hybridization (FISH) validates of MNA with *MYCN* (green) and D2Z (red) probes (C). Composition of the *MYCN* amplicon is examined with probes for *MYCN* (green) and *NAG* (red) (D). White arrows point out good examples of *MYCN*-amplified cells. White bar, 10 μ m.

3.1.3 Intratumoral heterogeneity in *MYCN* amplicon composition

Heterogeneity in *MYCN* amplicon size and composition has thus far not been reported in the same piece of a heterogeneous MNA neuroblastoma. The genetic composition of the *MYCN* amplicon was investigated by I-FISH with probes to *MYCN* and the adjacent gene *DDX1*. MLPA and SNP array data was again consulted for comparative reason. Data of the tumor presented in Figure 5 strongly indicates the existence of tumor cells carrying different *MYCN* amplicons in the same tumor piece. MLPA data revealed a large *MYCN* amplicon including *DDX1* and parts of *NAG* as well as an overrepresentation of the entire chromosome 2. SNP array data of the same tumor DNA confirmed the gain of chromosome 2 and clearly illustrated the *MYCN* amplification (Figure 5B). The detected amplicon appeared rather large spanning the 2p24.3→2p34.1 region with a size of approximately 8Mbp. Sequence analysis with the USCS genome browser (hg17) suggested the inclusion of *MYCN*-adjacent genes like *NAG*, *DDX1*, *SMC6*, and *SDCI* in the amplicon which have been reported to be coamplified in a core region identified in a number of MNA neuroblastoma [42]. While the average of both alleles (blue graph) portended a plateau similar to the MLPA data, a higher peak in the larger, red allele was identified which corresponded to *MYCN* specifically (Figure 5B, red arrow). Amplicon composition was further investigated by *MYCN/DDX1* I-FISH and confirmed the existence of tumor cells with the two amplicons in the same tumor piece (Figure 5 C). Tumor cells in the upper panel of Figure 5C carrying *MYCN/DDX1* coamplifications are marked with white arrows and contrasted the marked tumor cell with a “*MYCN*-only” amplicon in the lower panel. Although the definition of the border of the marked nucleus in the lower panel is again difficult, a clear imbalance with an estimated ratio of 16/5 between *MYCN* and *DDX1* signals is visible. The five *DDX1* signals show good correlation to *MYCN* probes and correspond well to the copy number of chromosome 2. Coamplification of the other, adjacent genes was not examined by I-FISH.

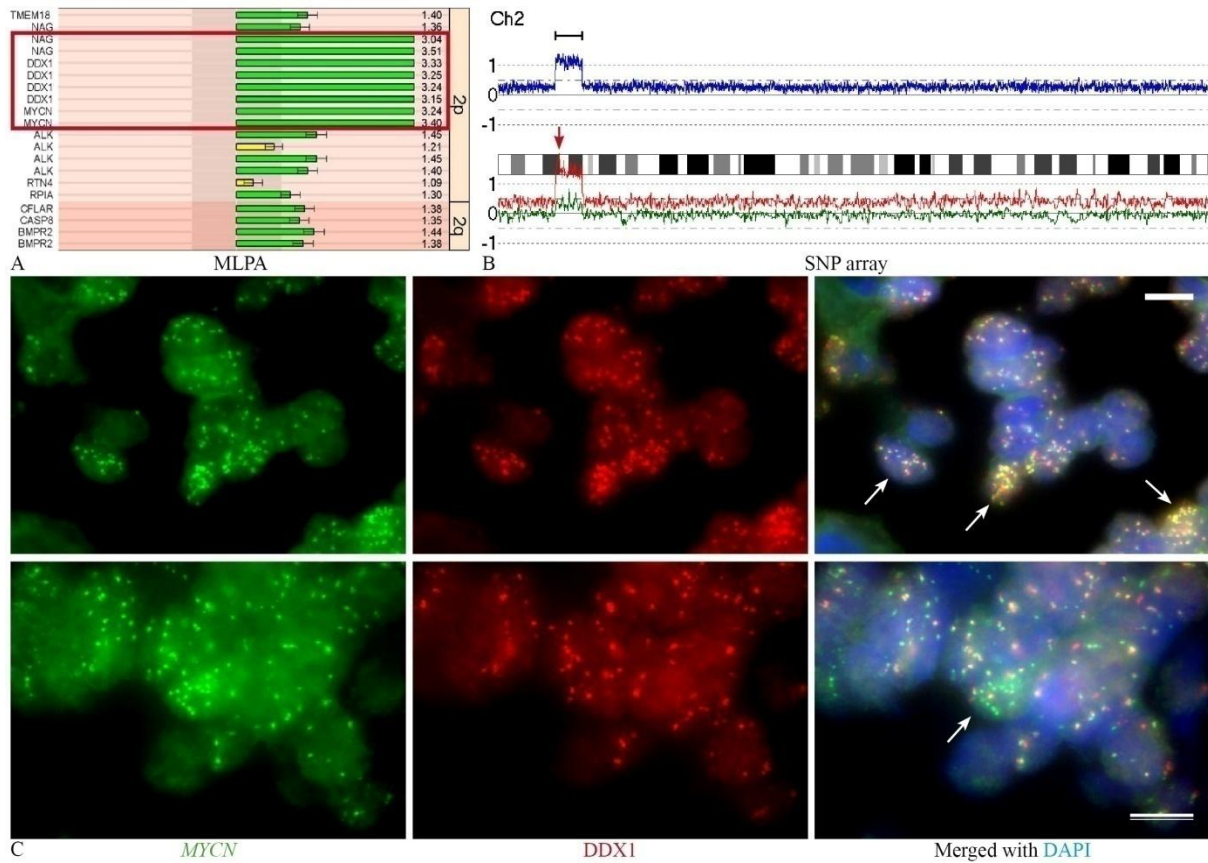


Figure 5: Heterogeneity in size and composition of the *MYCN* amplicon in a hetMNA neuroblastoma. (A) MLPA data of chromosome 2 shown with a red rectangle marking the amplified genes. In the single-chromosome view of SNP array data on chromosome 2 is displayed (B). The large amplicon is marked by the black bar and the *MYCN*-only amplification by the red arrow. The blue line illustrates the average copy number of both alleles; red (large) and green (small) lines depict allele based analyses. Chromosomes are represented by their cytoband information. (C) I-FISH stainings with probes for *MYCN* (green) and *DDX1* (red) were applied to illustrate the heterogeneous amplicon structure. *DDX1*-coamplified tumor cells are marked by white arrows in the upper panel. A cell carrying the "MYCN-only" amplicon is pictured in the lower panel. White bars, 10µm.

3.2 Genetic heterogeneity in hetMNA neuroblastoma

The role of the genetic background in the initiation of *MYCN* amplification in NB has in the past not been sufficiently studied and was examined only partially in homogeneously *MYCN*-amplified neuroblastoma [12]. To investigate whether a common segmental or chromosomal aberration in the tumor background is underlying the initiation of *MYCN* amplification can best be studied in hetMNA NB. For this purpose, we examined tumors with a varying number of MNA tumor cells in focal areas or scattered among unamplified tumor cells. In total, five patients with hetMNA were included in this study. According to the work up protocol of the INRG biology group [115], MNA was confirmed by *MYCN* I-FISH in at least one tumor piece of each patient. SNP arrays were selected to investigate chromosomal copy number alterations in a total of 13 tumor pieces. The following data focuses on the difference of segmental chromosomal aberrations, deletions and amplifications between tumor pieces and only partially at numerical chromosomal differences.

The standard genomic overview as obtained by the SNP array read-out and subsequent analysis with the CNAG software is shown for patient #1 in Figure 6. Heterogeneity for MNA was already visualized with *MYCN* I-FISH. The majority of NB cells showed no amplification while approximately one per cent of scattered tumor cells had MNA of up to 15-fold in reference to the copy number of chromosome 2. Since there was only one tumor piece of the patient available, investigation of heterogeneity was only possible within this piece. The DNA index for the tumor cells was not determined. Since CNAG draws the base line according to average copy number, the inference to tumor ploidy was difficult without other leads. Routine I-FISH stainings clarified the copy number of at least a few chromosomes. The application of the centromeric probe D1Z1 and the 1p subtelomeric probe D1Z2 showed cells with up to six balanced signals for both probes suggesting an average hexasomy for chromosome 1. Non-amplified tumor nuclei showed a balance of up to 8 copies of both arms of chromosome 2. Testing for chromosome 17 aberrations with probes for both p- and q-arm proved a predominantly unbalanced ratio with 4/5 and 6/7 signals per cell suggesting a potential 17p-deletion or 17q-gain. Based on the FISH data, we decided that the zero-line in the SNP array results corresponded to 6 copies of a chromosome. Another challenge in SNP array based analysis of heterogeneous tumors is the identification of different tumor cell clones with different single chromosome copy numbers and ploidies that contribute DNA according to

their percentages of the entire cell population. Our SNP arrays were limited to showing an average chromosomal copy number of the tumor cell population. Thus, the *MYCN* amplification (Figure 6, red arrow) was only vaguely visible in the analysis due to a low percentage of MNA tumor cells. It was also apparent that cells existed which carry a 2p-gain. Whether *MYCN* amplification and 2p-gain occurred in the same cell was not possible to be clarified satisfyingly. Furthermore, chromosome 4 showed two gains, the first at the telomere of the p-arm (4pter→4p16.1) and the second close to the centromere on the q-arm (4q11→4q12), as well as an amplification corresponding to *CXX4* gene (blue asterisk). This gene is a negative regulator of the Wnt signaling pathway. Chromosome 6 had two break points, the first one at 6q12 and the second at 6q15. While 6pter→6q12 including the centromere was on average septa- to octasomic, the part between 6q12 to the second break point at 6q15 was only hexasomic. The region 6q15→6qter was even tetrasomic.

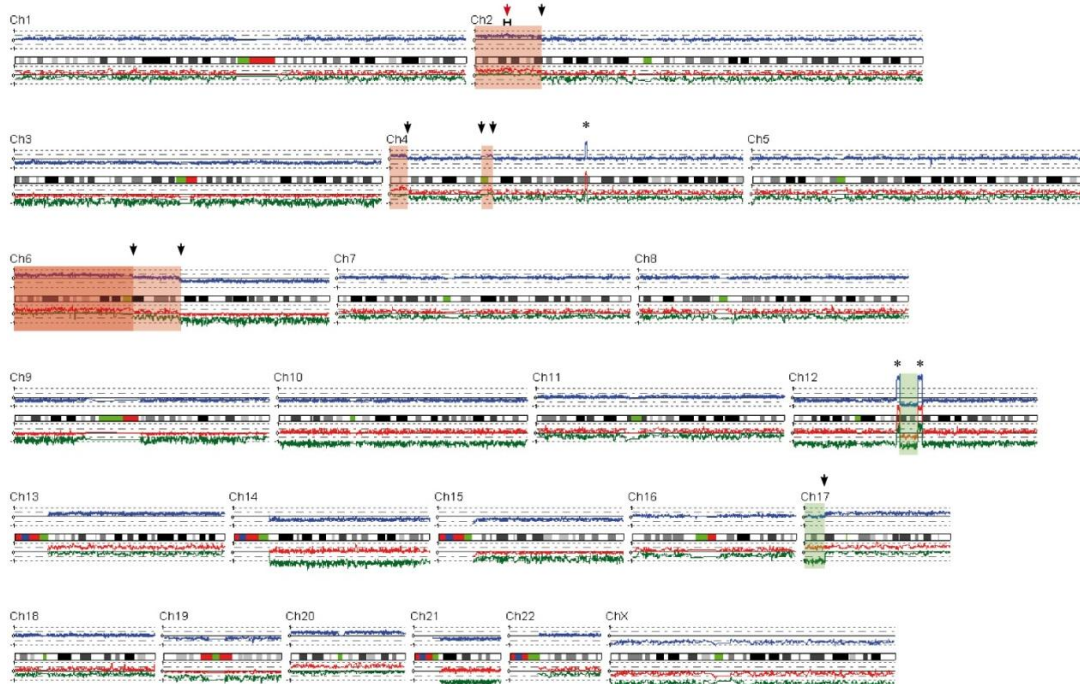


Figure 6: All genome view of SNP array data provided an excellent overview of genomic aberrations in tumor samples. SNP array data from patient #1 is shown in the all-genome-view generated. The blue line illustrates the average copy number of both alleles; red (large) and green (small) lines depict allele based analyses. Chromosomes are represented by cytobands information. The red arrow points at the *MYCN*-location on chromosome 2, while black arrows mark chromosomal break points and asterisks other amplifications. For better visualization of segmental aberrations, gains are highlighted in transparent red and losses in transparent green.

Chromosome 12 appeared to be tetra- to pentasomic but two regions were displayed with very strong hybridization signals indicative of amplified sequences. These regions flank a fragment which was completely lost in the smaller allele and showed reduced hybridization in at least two copies of the 3 to 4 copies of the larger allele. Interestingly, the more terminal amplicon included the *Mdm2* gene locus at 12q15. *Mdm2* is proven to be an important repressor of the transcriptional activity of the p53 tumor suppressor and induces p53 degradation [119]. Whether these amplifications and the loss were actual genomic alterations remains to be tested by FISH with appropriate DNA probes or other methods. A partial loss of the p-arm of chromosome 17 was also detected with a break point at 17p12. It is clearly visible that only the smaller, green allele was affected by the loss of the fragment 17pter→17p12. The larger, red allele remained intact leading to an overall ratio of approximately six copies of the 17p-arm versus eight copies of the rest of the chromosome. When compared to the 17p/q- I- FISH results, the assessment of the ratio seemed to be accurate.

Touch preparations were sent in for routine FISH diagnostics of the tumor of patient #2. Two distinct areas were identified with MNA NB cells, a large area with 5000 cells and an estimated percentage of 30-40% MNA tumor cells and a smaller area of 2000 cells and roughly 10% MNA. The copy number of *MYCN* was increased of up to 20-fold in reference to the largely trisomic chromosome 2. Few, diffuse MNA cells were also found in close proximity to the two focal areas. Touch preparations and cryosections from four tumor pieces labeled A to D also showed on average tri- to pentasomies for chromosome 2 but no MNA cells were detectable by *MYCN*-FISH (data not shown). Correspondingly, none of the tumor pieces revealed *MYCN* amplification in SNP array analysis (Figure 7). While tumor pieces A to C only showed numerical aberrations, tumor piece D additionally presented a 17pter→17p11.2 deletion. The break appears to have occurred with higher incidence in the larger, red allele, and only to a minor extent in the smaller, green allele of a few tumor cells.

On average, all four pieces were pentasomic for chromosome 17 with tumor D having lost the terminal region of the 17p-arm. Furthermore, SNP array data confirmed disomy of chromosome 11 but tumor piece C showed a uniparental isodisomy with the small allele entirely lost and the other one duplicated (data not shown) adding another level of heterogeneity to the tumor of patient #2. The unmarked deletion visible in pieces B to D was likely an artifact from the procedure with no known gene sequence affected.

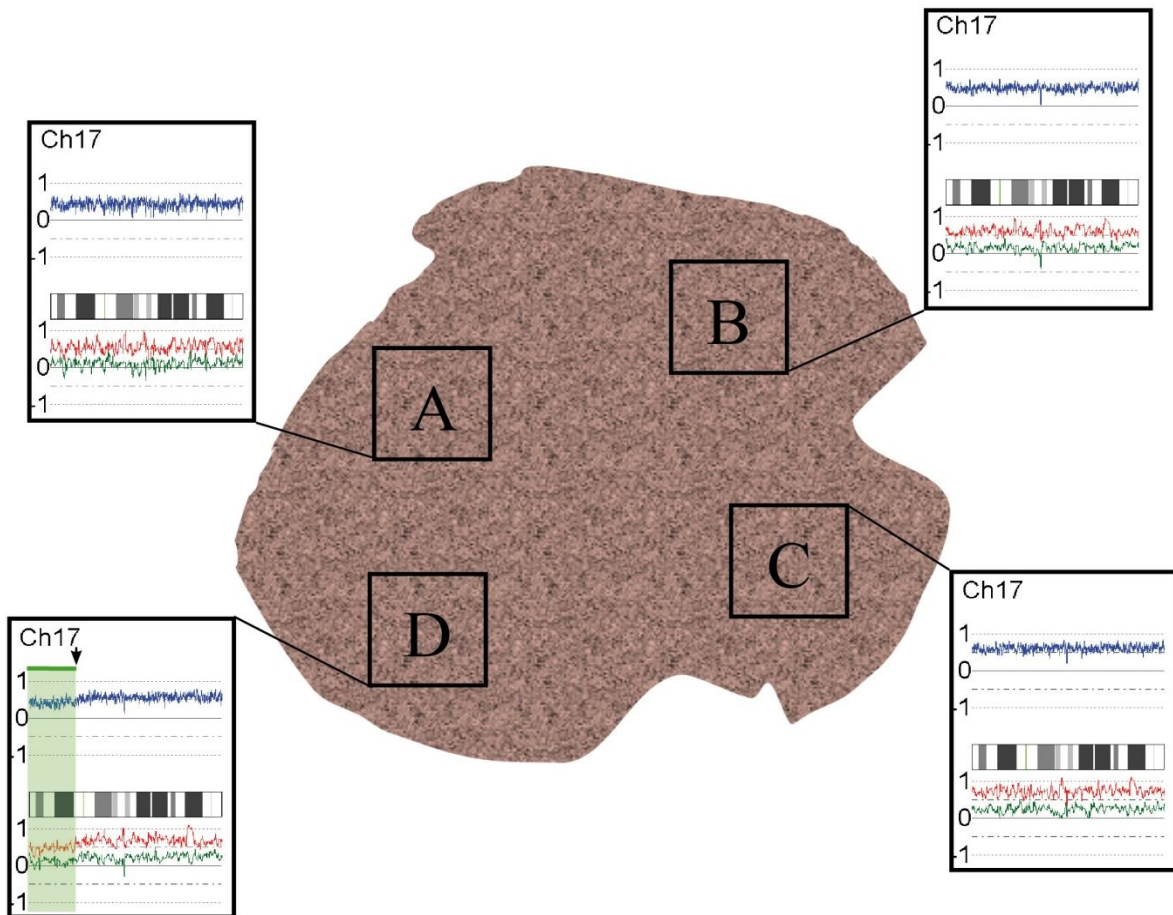


Figure 7: One out of four tumor pieces from patient #2 showed a 17p- deletion. SNP array analysis was done on the four tumor pieces of patient #2 labeled A to D. Chromosome 17 is shown in the single-chromosome-view. The blue line illustrates the average copy number of both alleles; red (large) and green (small) lines depict allele based analyses. The chromosome is represented by the cytoband information. For better visualization of the 17p segmental aberrations, the loss is highlighted in transparent green and the black arrow marks the break point.

The molecular-cytogenetic I-FISH report for patient #3 was based on two pieces A and B of the same tumor. The report stated that MNA was only detected in tumor piece B with numerous cells carrying a 15- to 30-fold increased copy number of *MYCN*. Piece A and a biopsy, which was sent a week in advance of the tumor, did not confirm the existence of MNA. However, tumor piece A was later sectioned again for the investigation of heterogeneity in *MYCN* amplicon composition by FISH and eventually revealed MNA in a few scattered cells. MNA heterogeneity was thus already visible in the FISH results from both tumors. SNP array analysis confirmed the heterogeneity. With a DNA index of 1.55, both tumor pieces showed the same extensive numeric chromosomal aberrations (NCA) including 42

a trisomy of chromosome 2 which is visible in Figure 8. Segmental chromosomal aberrations at the applied array resolution were not detected. The *MYCN* amplicon was only detectable in tumor piece B owing to the high percentage of MNA NB cells in the B piece. The size of the amplicon was rather large spanning the 8Mbp region 2p24.3→2p34.1 and included adjacent genes like *NAG*, *DDX1*, *SMC6*, and *SDC1* which were shown to be coamplified in a core region of a number of MNA NB tumors [42]. Interestingly, a higher peak in the larger, red allele was identified which corresponded to *MYCN* specifically. The detection of the peak and the plateau in the same tumor piece suggested amplicon heterogeneity with a small, *MYCN*-only besides the large amplicon containing the coamplified genes listed above. Amplicon composition was investigated by *MYCN/DDX1* I-FISH and confirmed the existence of tumor cells with the two amplicons (Figure 5). Coamplification of the other, adjacent genes was not examined by I-FISH.

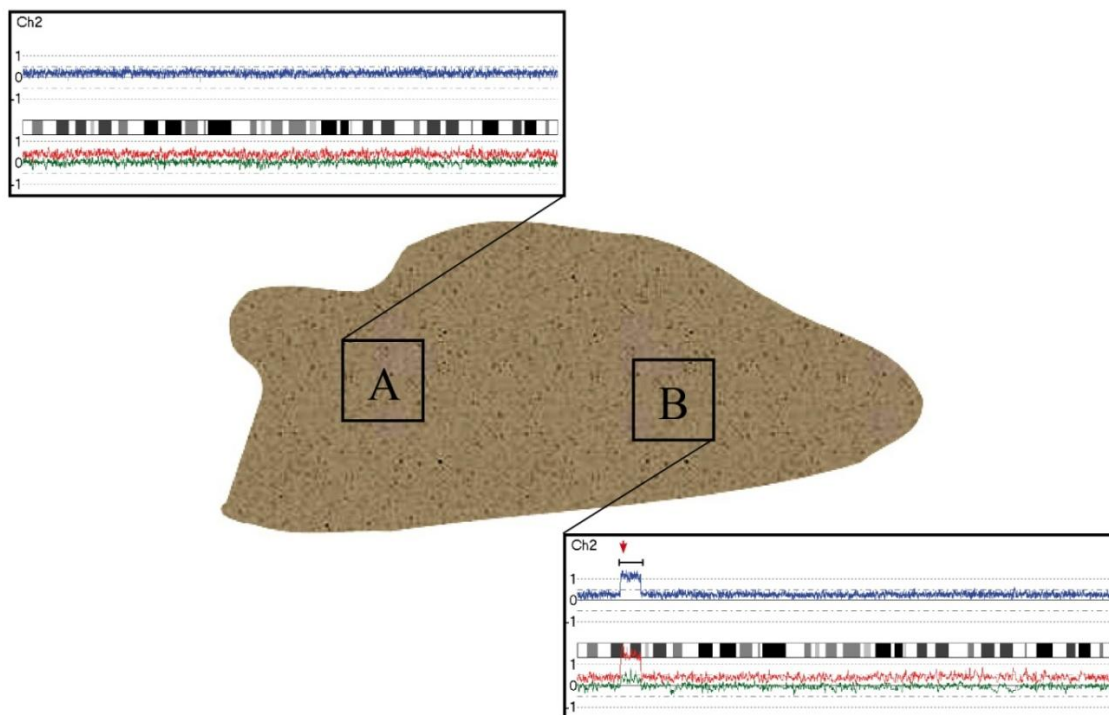


Figure 8: MNA heterogeneity was detected in the two tumor pieces of patient #3. Pieces A and B were screened for chromosomal aberrations with SNP arrays. The single chromosome views are shown in the black boxes for chromosome 2. The *MYCN* amplicon is marked by a black bar and the location of *MYCN* gene indicated by the red arrow. The blue line illustrates the average copy number of both alleles; red (large) and green (small) lines depict allele based analyses. The chromosome is represented by its cytoband information.

Four tumor pieces labeled I to IV were screened of patient #4. Each of the touch preparations that were used for I-FISH routine diagnostics of the four pieces revealed MNA tumor cells. While the touch preparations of pieces II to IV only showed a sparse number of diffuse amplified cells, tumor piece I revealed focal cells with a two to 15-fold increase of *MYCN* in reference to a tri- to tetrasomic chromosome 2. Furthermore, I-FISH with probes D1Z1 and D1Z2 proved segmental imbalance for chromosome 1, which suggested a 1p deletion in the majority of tumor cells of pieces II and IV and to a lesser degree in the touch preparation III. Tumor cells from piece I, on the other hand, appeared balanced for both probes. The patient report also mentioned the non-existence of a segmental aberration of the tetrasomic chromosome 17. SNP array analysis of the four tumor pieces confirmed to a large extent the patient report (Figure 9). Tumor piece I was the only one with a detectable *MYCN* amplification, while the other pieces showed no sign of amplification due to the low abundance of MNA tumor cells. On the contrary to the patient's FISH report, the 1p loss was not only visible in three but in all four pieces. The aberration was most prominent and clear cut in tumors II and IV. Breakpoints in pieces I and III were less clear to identify and the aberrations were less defined indicating a low percentage of 1p-aberrated cells. Interestingly, the 1p-aberrations were of different size in the tumor pieces. At least two distinct breaks were detectable. While tumor cells in piece II carried a 1pter→1p22.2 loss, NB cells in piece IV showed a 1pter→1p21.2 loss. The other two pieces potentially shared both clones in low and different quantity which might explain the smooth decrease in signal and the more difficult identification of the actual chromosomal break point. Data to confirm this assumption was not collected. Furthermore, data for chromosome 3 of tumor II indicated a segmental gain of the region 3q13.31→3qter which likely affected both alleles. A comparable gain was not identified in the other three tumor pieces. Additionally, an 11q-loss of primarily the larger allele was detected in piece IV and unmatched in the other pieces. Numeric chromosomal aberrations for a number of chromosomes were also detected and were consistent in all four pieces. According to I-FISH data, tumor piece IV was tetrasomic for chromosome 1 while the other pieces were trisomic (data not shown).



Figure 9: Four tumor pieces of patient #4 revealed extensive genetic heterogeneity. SNP array data of patient #4 is shown in an overview of selected single-chromosome-views generated with the CNAG 3.0 software. Chromosomes 1, 2, 3 and 11 were selected because of heterogeneous genetic aberrations. The blue line illustrates the average copy number of both alleles; red (large) and green (small) lines depict allele based analyses. Chromosomes are represented by their cytoband information. The red arrow points out the genomic *MYCN* location, while black arrows mark chromosomal break points. For better visualization of segmental aberrations, gains are highlighted in transparent red and losses in transparent green.

The case of patient #5 was different from the other four patients. Two different tumor pieces were screened for heterogeneity, the initial tumor and a resection during treatment (D.T.). The patient report of the near-triploid initial tumor with a DNA index of 1.49 included the detection of a 1p-deletion, three centromeres versus one or two p-telomeres, by FISH in the majority of tumor cells interspersed with a few cells without deletion. In the respective touch preparation of the tumor, very few cells (~0.05%) were identified by I-FISH to carry an *MYCN* amplification of up to 30-fold. An aberration of chromosome 17 was not detected. PCR was used for the investigation of the loss of heterozygosity of chromosomal region 1p36.6 in the D.T. - tumor and did not confirm the loss detected in the initial tumor. MNA

was also not detectable by southern blot analysis with a *pNbl* probe. *MYCN* I-FISH was not conducted on this piece.

SNP array data on both tumors revealed contradictory results to the FISH report (Figure 10). Heterogeneity of MNA was verified, but not as suggested by the molecular-cytogenetic report. While in the initial tumor MNA was absent on the SNP array, a clear peak was detected in the D.T. - tumor piece. Additionally, the 1p segmental loss seen by I-FISH in the majority of cells in the initial tumor was not confirmed by SNP array. Both tumors displayed a gain of a ~1000kb region (17q21.31→17q21.32) on chromosome 17. Among other genes, this segment includes *WNT3* and *WNT9B* which are two genes of the WNT gene family and are implicated in oncogenesis [120]. The gain also included *MAPT*, a gene with common numeric variants (CNV) in humans. A consistent deletion was also detected at 20p12.1 on chromosome 20 but did not include a known gene. This site was also compared to the UCSC data base of genomic variants and was identified as a CNV as well. Reference material from the patient was not tested to differentiate between CNV- or tumor-specificity.

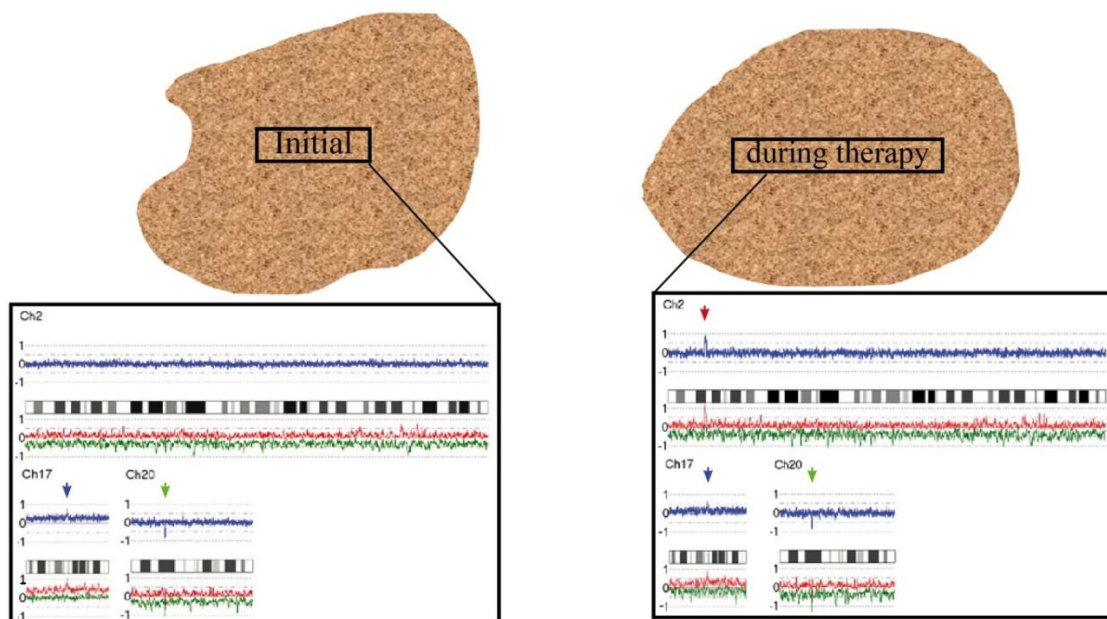


Figure 10: Heterogeneity of MNA was detectable in the initial tumor and in the resected tumor during treatment. The two pieces of patient #5 were screened for chromosomal aberrations with SNP arrays. Single-chromosome-views are shown for chromosome 2, 17, and 20. The *MYCN* amplicon is indicated by a red arrow. The amplification on chromosome 17 is marked with a blue arrow and the deletion on chromosome 20 with a green arrow. The blue line illustrates the average copy number of both alleles; red (large) and green (small) lines depict allele based analyses. The chromosome is represented by its cytoband.

An overview of the SNP array data of each of the 13 tumor pieces is given in Figure 11. Since all tumors were at least near-triploid, every sample carried a number of whole chromosomal gains marked by the light pink color. Except in the potentially hexaploid tumor of patient #1, chromosome 19 was the only chromosome which appeared disomic. Chromosomes 1, 2, 5, 6, 7, 8, 12, 13, 17, 18, and 22 were all overrepresented in the 13 tumor pieces. A common segmental aberration, however, was not identified at the resolution of the applied SNP arrays and is thus unlikely to initiate *MYCN* amplification. Due to the heterogeneity of the tumor cells in the pieces used for DNA extraction and the nature of SNP arrays, a conclusion on potential combinations of certain aberrations in a single cell cannot be drawn.

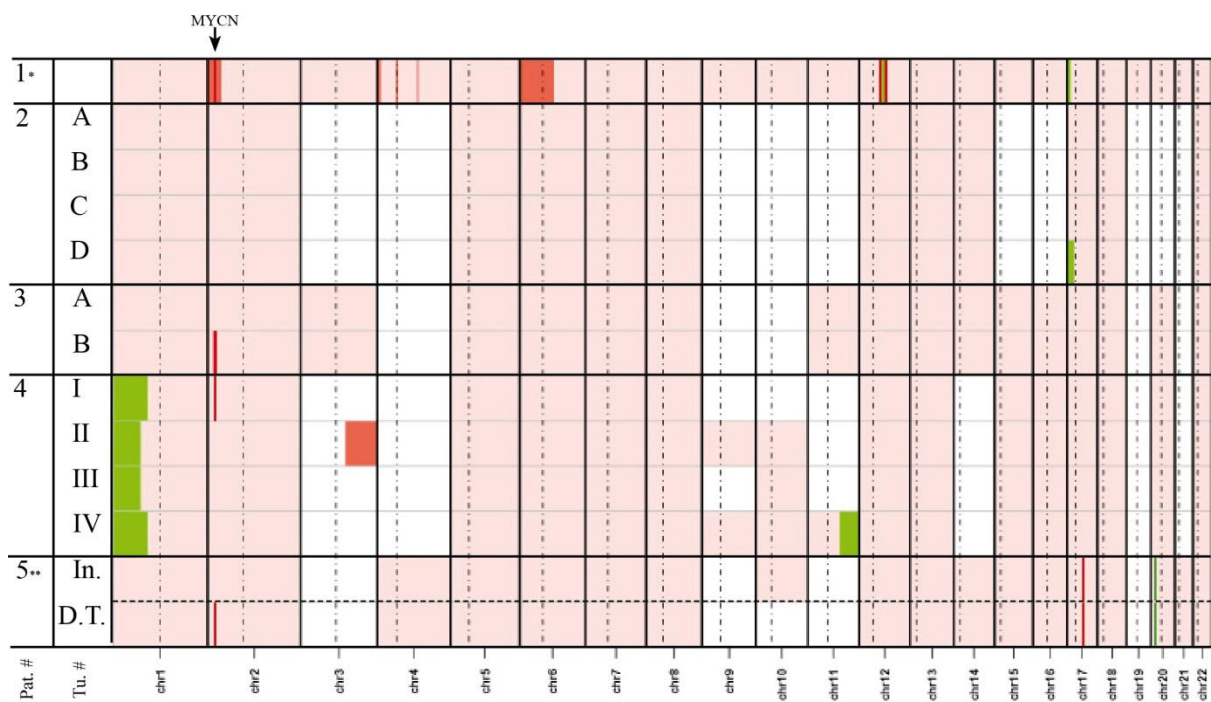


Figure 11: Heterogeneous tumors show no common segmental aberration. Affymetrix GeneChip® Human Mapping 250K Nsp Arrays were used to investigate the genetic background of hetMNA NB. The different tumor samples were compared to one another. The light pink color marks entire overrepresented chromosomes, light red depicts gained segmental aberrations and dark green lost segmental aberrations. The dark red bands illustrate amplifications and green bands deletions. The bands for the *MYCN* amplicon and other single-gene aberrations are slightly broadened for better visualization and do not resemble the actual size of the amplicon. Since the analysis of the array data is based on a diploid karyotype, white color indicates disomic chromosomes. * The tumor of patient #1 showed strong heterogeneity in the *MYCN* I-FISH results. ** The two compared tumor pieces of patient #5 were primary and during-therapy. Pat. # patient number; Tu. # tumor number; In. initial; D.T. during therapy

3.3 Genetic instability involvement in *MYCN*- amplification

DNA double strand breaks were reported to lie at the bottom of gene amplification [121]. However, the role of DSBs in the establishment of *MYCN* amplification in NB tumors has so far not been clarified sufficiently. In these experiments, we conducted first steps to examine whether DSBs are underlying amplification of *MYCN*. By immunofluorescence detection of γ H2AX at the loci of DSBs and subsequent *MYCN* I-FISH, we investigated the correlation of unrepaired DSBs and *MYCN* amplification on sections of NB tumors. Our prime interest lay in heterogeneous tumors which are best-suited to discriminate DSB-occurrence in *MYCN* amplified from non-amplified tumor cells in the same tissue section. As references, we included homogeneous neuroblastoma in our study that showed NCAs-only, no MNA but SCAs and NCAs and tumors with classic MNA and SCAs in their MLPA analysis.

The staining pattern of γ H2AX on hetMNA tumor cryosections revealed an overall independence of *MYCN* amplification and the presence of DNA double strand breaks in the same tumor cell (Figure 12). Two tumor pieces of a patient's neuroblastoma (Figure 12A and B) were chosen that revealed only numeric chromosomal aberrations in the background of a *MYCN* amplification in the one tumor piece (Figure 12B) by MLPA and SNP array analysis (see also Figure 8 for excerpts of the SNP array data). Frozen sections of both pieces generally displayed a diffuse γ H2AX staining in a few tumor cells which varied from a very weak pan-nuclear staining to a strong granular staining with some distinct foci. For one, the displayed images give the impression that the γ H2AX staining pattern is unclear and the occurrence of DSBs is neither connected to tumor cells carrying NCAs with normal *MYCN* copy number (red arrows) or with amplification(red arrow heads). Furthermore, tumor cells of both types were detected without any γ H2AX staining (white arrow). It also appeared as if most *MYCN* amplified tumor cells displayed only a very weak signal or were even negative for γ H2AX.

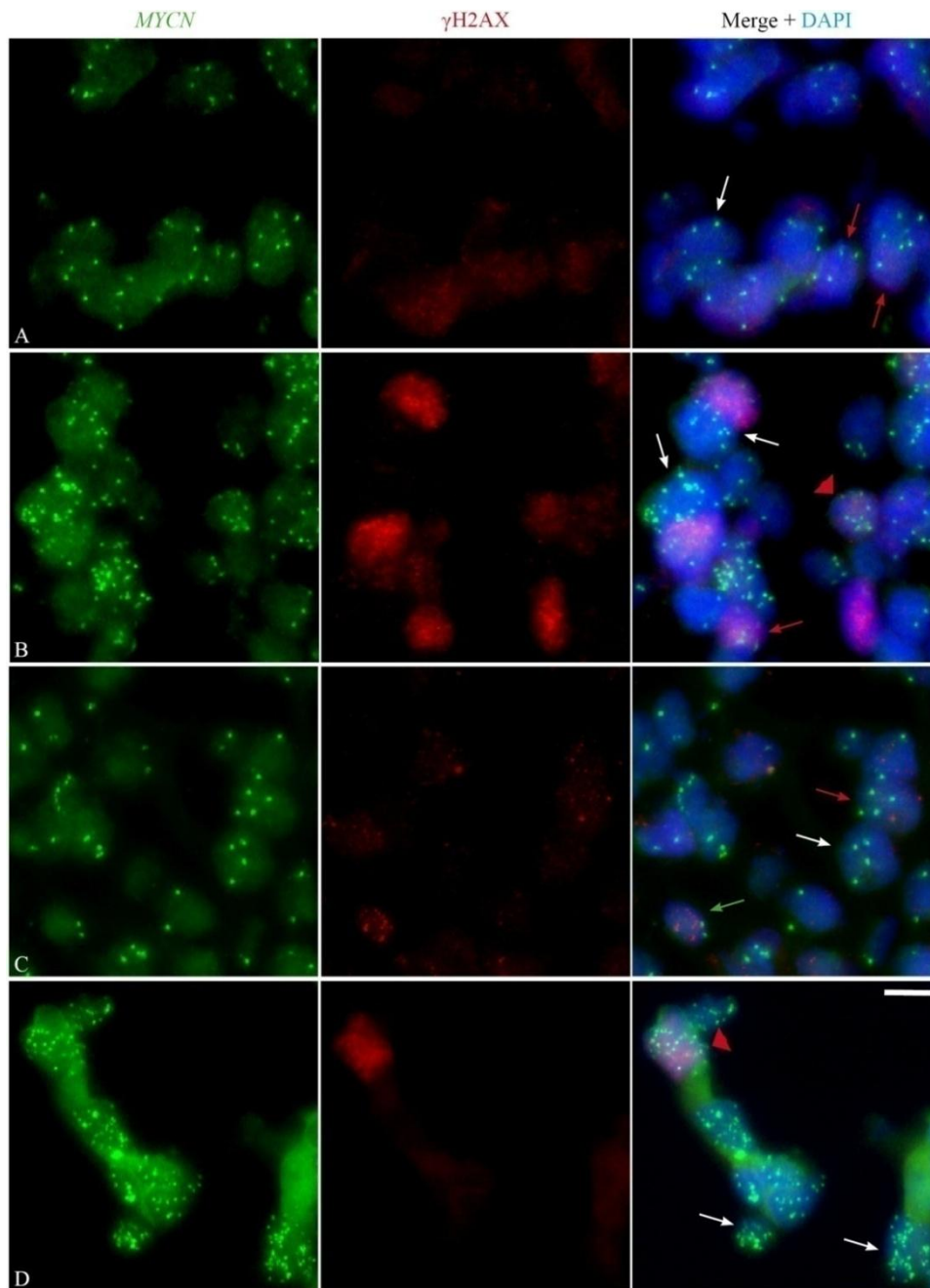


Figure 12: *MYCN* amplification only partially correlates with the occurrence of DNA double strand breaks in hetMNA neuroblastoma. Images show combined stainings of FITC-labeled *MYCN* I-FISH (left column) on Cy3-labeled γ H2AX prestained cryosections (middle column) of hetMNA tumor pieces. Merged images of FITC, Cy3 and DAPI are depicted in the right column. Stainings of two tumor pieces of the same hetMNA neuroblastoma with NCA are displayed; one piece with a very low percentage or no MNA cells (**A**), the other with a high percentage of MNA cells (**B**). Two pieces of a hetMNA tumor with SCA are depicted in the lower two rows, one with no detectable MNA cells (**C**) the other with large areas of amplified cells (**D**). White arrows point at tumor cells with little or no γ H2AX staining, red arrows at tumor cells with γ H2AX staining, the arrow heads at double-positives, and the green arrow at a disomic cell of unknown cell type. White bar, 10 μ m.

The two lower panels of Figure 12 feature stainings of a hetMNA tumor with segmental chromosomal aberrations (see also Figure 9 for excerpts of the SNP array data). The section in Figure 12C of the MNA-poor tumor piece displays a number of tumor cells without *MYCN* amplification that presented γ H2AX foci (red arrow) in close proximity to negative cells (white arrow). Foci were also detected in disomic cells of unknown type (green arrow). The MNA-rich tumor piece (D) was almost devoid of γ H2AX-positive cells with a few exceptions that exhibited a pan-nuclear staining (D, red arrow and red arrow heads). However, the majority of *MYCN*-amplified tumor cells were negative for the phospho-histone staining.

In order to obtain an impression of the overall genomic instability and the incidences of γ H2AX-positive cells in a tumor, single images were stitched together to a section overview. Figure 13 displays the two previous heterogeneous neuroblastomas (Figure 13A/B and C/D) in comparison to homogeneous neuroblastoma reference material (Figure 13E/F, G/H and I/J). As aforementioned, the homogeneous tumors were assigned to three different categories: NCAs-only, NCAs and additional SCAs, and classic MNAs with segmental and numeric chromosomal aberrations. At least three tumors of each category were examined for their γ H2AX staining pattern. The selected hetMNA tumor pieces both featured high frequencies of *MYCN* amplified cells detected by I-FISH. MNA was also traceable in each case by MLPA and SNP array analysis (see also Figure 5 and Figure 3). The hetMNA tumor with only NCAs in the genetic background of MNA (A/B) demonstrated a heterogeneous staining pattern with a higher number of γ H2AX-positive cells in comparison to the tumor with additional SCAs (C/D). Although a few cells displayed a stronger granulation (B), the overall staining in the two selected pieces was diffuse and occasionally pan-nuclear. In the tumor representing neuroblastoma with NCAs-only, very few cells stained for γ H2AX (E/F). Additionally, a number of these cells were of unidentifiable cell type and proved to be disomic for *MYCN* (F, green arrow). Neuroblastoma with segmental aberrations displayed a more extensive staining pattern. Again, tumor cells were either negative or positive for γ H2AX and some cells of potential stromal character also exhibited the staining. While the difference in the overall intensity of the γ H2AX staining between tumors with NCA-only and those with segmental aberrations was not always striking, “classic” MNA neuroblastoma always presented a discriminable, unique staining. A high number of *MYCN* amplified cells showed a cloudy, diffuse γ H2AX staining largely different from cells of the other tumor categories. A few amplified cells evidenced a very strong pan-nuclear staining (Figure 14).

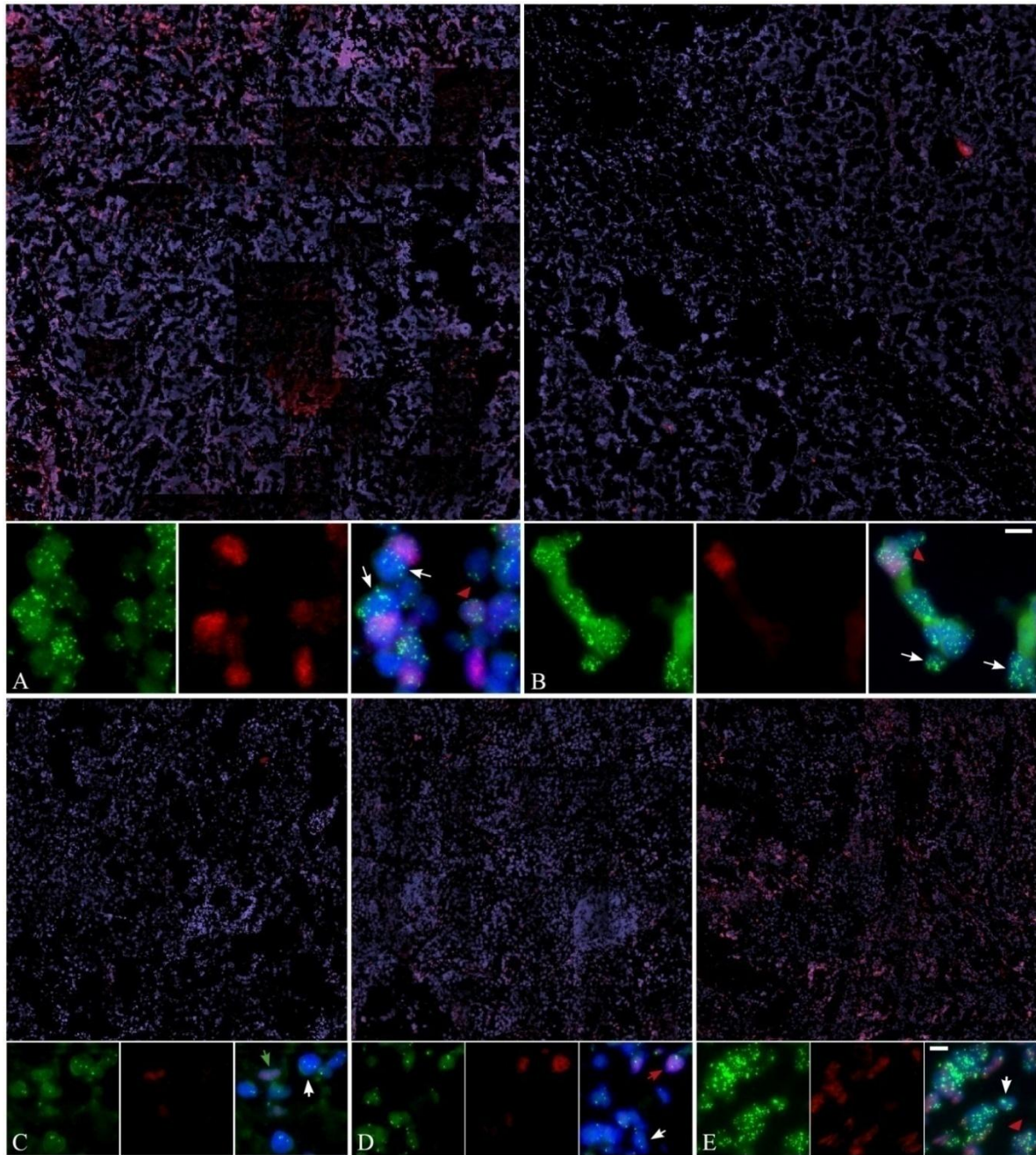


Figure 13: γ H2AX staining pattern is heterogeneous in different hetMNA neuroblastoma and compares weakly to homogeneous tumors. Overview images and the detailed images in the panel below are always from the same tumor. Overviews are stained for γ H2AX and counterstained with DAPI. In the panel of the detailed images, *MYCN*-FISH is green (left image), γ H2AX immunostaining is red (middle image). Merged images (right image) are counterstained with DAPI (blue). Correlated stainings are displayed for γ H2AX and *MYCN* amplification in a hetMNA tumor with NCA (**A**) and a hetMNA tumor carrying SCAs (**B**). References of *MYCN* I-FISH and γ H2AX immunostaining on sections of homogeneous NBs with NCA without MNA (**C**), SCAs without MNA (**D**) and SCAs with classic MNA (**E**) are given below. Red arrows denote positive and white arrows negative tumor cells for γ H2AX staining. Red arrow heads identify double-positive cells. The green arrow marks a γ H2AX positive cell of unknown cell type. White bars, 10 μ m.

Interestingly, the “classic” MNA tumors also showed an overall heterogeneous γ H2AX staining pattern with focal areas with a majority of positive tumor cells and areas completely devoid of or with only single positive cells Figure 14.

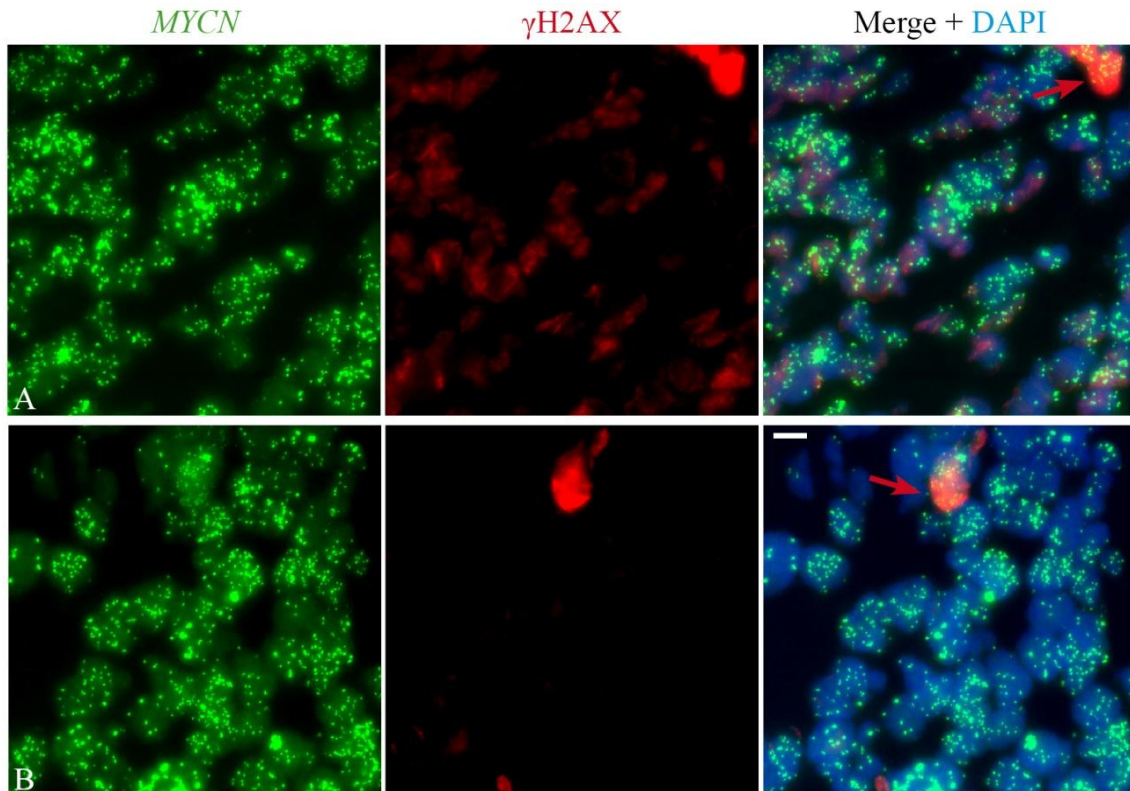


Figure 14: “Classic” MNA neuroblastoma display areas without and with strong γ H2AX immunostaining. Images show combined stainings of FITC-labeled *MYCN* I-FISH (left column) on Cy3-labeled γ H2AX prestained cryosections (middle column) of MNA tumor pieces. Merged images of FITC, Cy3 and DAPI are depicted in the right column. Red arrows mark tumor cells with strong γ H2AX positivity. Images were taken at 40-fold magnification with fixed integration times. White bar, 10 μ m.

One of the examined tumors with SCAs carried a loss of distal 11q which was detected by MLPA (Figure 15). Based on the MLPA readout (Figure 15A), it can be said that at least a segment starting with the gene *CNTN5* at 11q22.1 to *THY1* at 11q23.3, possibly to the terminus of chromosome 11, was continuously lost in this tumor. Although the MLPA kit lacks probes for the *H2AFX* gene locus at 11q23.3 specifically, it can be assumed by the losses of the proximal gene *HMBS* and the distal gene *THY1* that *H2AFX* was also lost. The *ATM* gene, which encodes the ATM kinase that phosphorylates H2AX upon DNA double strand break recognition, was additionally included in the lost segment. Nonetheless, the

tumor displayed γ H2AX-specific staining in a number of cells (Figure 15B/C). The type of these cells, however, remained unclear since most of them proved to be disomic in *MYCN* I-FISH and were thus not unambiguously identified as tumorigenic (red arrows). Well-defined trisomic cells, on the other side, stained largely negative (white arrows). Despite the segmental loss of 11q, a number of cells show no implication on DNA double strand break signaling or repair. However, an additional neuroblastoma-specific staining needs to be conducted to clarify the nature of these γ H2AX-positive cells.

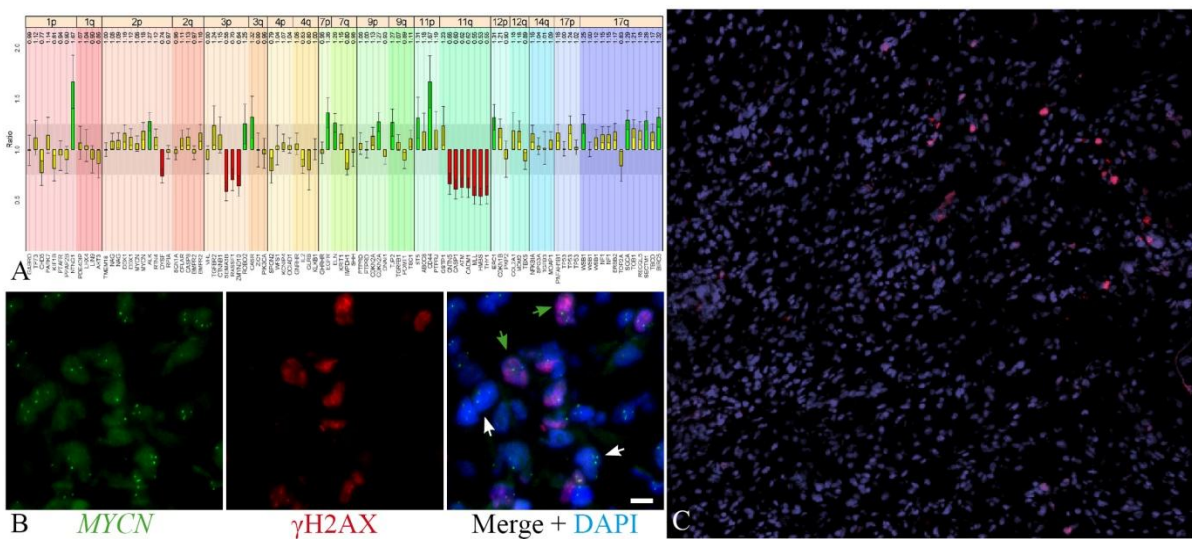


Figure 15: Neuroblastoma with 11q-loss shows substantial γ H2AX staining. MLPA displays prominent 11q deletion including the *H2AFX* gene locus (A). The detailed images (B) in the panel below and part of section overview (C) are from the same tumor. *MYCN*- FISH is green, γ H2AX immunostaining is red and DNA is blue for all images. Images were taken at 40-fold magnification with fixed integration times and stitched together for the overview. Black rectangle marks the lost segment on chromosome 11. White arrows mark examples of γ H2AX negative tumor cells and green arrows positive cell of unknown cell type. White bar, 10 μ m.

4 Discussion

The accurate categorization of neuroblastoma is a crucial step in the decision making process for the appropriate treatment approach for a patient. Treatment strata are increasingly sharper formulated for homogenous NB [122]. The risk stratification for a potential outcome of this subgroup is more predictable. Up to this point, the clinical relevance of heterogeneity in NB remains largely non-elucidated and the tumors are difficult to assign to specific risk groups and outcome. Amplification of the *MYCN* oncogene is one of the standing markers for the detection and diagnosis of an aggressive subset of neuroblastoma with dismal prognosis [9, 17, 123]. Contradictory results were recently published on the ability to determine tumor progression of a few MNA cells [48]. On the other side, MNA in homogeneously amplified tumors is considered to induce rapid tumor progression possibly contributing to metastatic growth. A major area of uncertainty in homogenous as well as heterogeneous MNA neuroblastoma is the emergence of *MYCN*-amplification in tumor. While the actual event of amplification is regarded to occur in a episomal model [40 (in press)], the elicitor has not been found yet.

4.1 Detecting heterogeneity in neuroblastoma

In this report, we assessed the performance of different techniques in the identification of *MYCN* amplification in hetMNA tumors. Knowing the tumor cell content in a patient sample is crucial for the correct interpretation of results obtained by methods other than single-cell approaches. DNA, RNA or protein extraction is the initial step for PCR or array-based examination of samples. Without selection of specific areas by microdissection, for instance, a large number of cells is generally processed which leads in subsequent molecular tests to averaged results for a cell population. There is also a good chance that a high percentage of non-tumor cells can distort the data and identification of the genetics of a tumor clone can be complicated or even impossible. Assessment of tumor material is usually done with a pathologist on the grounds of hematoxylin and eosin stainings of sections. Additionally, the International Neuroblastoma Risk Grouping (INRG) biology committee allows the estimate of

tumor cell number to be based on I-FISH in certain NB cases [115]. Furthermore, the committee has set the required tumor cell content to more than 60% for most molecular studies and to more than 20% for ploidy measurement. BAC probes are generally used to investigate numeric aberrations of chromosomes, which are characteristic for a wide range of NB.

Our results on a total of 13 hetMNA tumor pieces from 5 patients confirmed that the histological workup of a tumor sample, the way it is done by pathologists with hematoxylin and eosin staining, is not sufficient to detect *MYCN* heterogeneity in NB. Morphologically, there is frequently no visible difference between homogeneous and heterogeneous tumor cells within the same tumor. *MYCN*- FISH is the only method for detecting amplification on a cellular basis and can lead to the confirmation of *MYCN* copy number heterogeneity already by itself. I-FISH with probes for the two respective chromosome arms can furthermore visualize a different form of heterogeneity by detecting segmental and numerical aberrations in tumor cells. In addition, MLPA is routinely performed on tumor DNA since a good overview of all relevant aberrations in NB can be obtained rather quickly. We also included SNP array-based analysis of the same DNA pool in our comparison. Our results clearly prove an advantage of I-FISH over both other methods in terms of detecting heterogeneous MNA. Since MLPA and SNP arrays are based on DNA analysis of many thousand tumor cells, the results only depict the average cell. As soon as the percentage of *MYCN* amplified cells is below a certain threshold – 60% is the threshold for tumor cells versus normal tissue – and the *MYCN* copy number per cell is rather low, a detection of MNA in the background of other tumor cells is impossible. *MYCN* I-FISH combined with a reference probe like D2Z showed the required sensitivity to detect single amplification events in well-permeabilized tumor cryosections. On the downside FISH is more time- and money- consuming and thus not suited to study the genetic background in detail in a hetMNA NB. However, we can confirm that the demand of the INRG Biology Committee to conduct *MYCN* I-FISH applies to heterogeneous MNA tumors and is absolutely necessary for single cell detection [115]. Genomic approaches like MLPA or array-based techniques are not sufficient to diagnose hetMNA NB and need to be combined with *MYCN* I-FISH.

4.2 Heterogeneity in amplicon composition

As aforementioned, genetic heterogeneity in neuroblastoma can assume different manifestations and heterogeneous *MYCN* amplification is one of them. Another form of is the number of amplicons per tumor cell. Episomal amplification of NUP214-ABL1 fusion gene in T- cell acute lymphoblastic leukemia (T-ALL) confers oncogenicity similar *MYCN* in neuroblastoma [124]. Due to the absence of a centromeric structure, the episome segregates unequally during mitosis and establishes a heterogeneous pattern in the tumor cells [36, 124]. Analogously, the *MYCN* amplicon in NB has also been observed to divide disproportionately during cell division. Whether this imbalance in amplicon number has any relevance for progression and prognosis of the tumor cannot be said.

Reports on heterogeneity in amplicon composition in the same NB tumor piece have not been published to our best knowledge. However, our data strongly supports the presence of different amplicons in the same hetMNA NB tumor (Figure 5). According to the detected amplicon size by MLPA, the majority of tumor cells showed a clear *DDX1* coamplification. Additionally, single cells were found to display a clear imbalance of signals for *MYCN* and *DDX1* suggesting a smaller amplicon without coamplifications of the *DDX1* gene. Interestingly, the two amplicons were also picked up by SNP array analysis in form of a plateau for the larger amplicon and a smaller, higher peak encompassing only the *MYCN* locus in one of the alleles. At the moment, we can only speculate about the emergence of the two different amplicon compositions. The coamplification pattern in a *MYCN* amplicon has shown extraordinary resistance to variability even during and after therapy [125]. However, an evolution of the *MYCN* amplicon cannot be dismissed per se. Since the most selective pressure is on the *MYCN* oncogene itself, a loss of the other genes in the amplicon would not lead to a disadvantage in proliferation and survival of the cells. Hence, a rearrangement is certainly possible. Another explanation would be the induction of *MYCN* amplification in two distinct cells of the same heterogeneous tumor. Whether it is assumed that either hetMNA neuroblastomas have a certain proneness to *MYCN* amplification or initiation is a result of chance, the possibility that two different amplicons can arise independently in the same tumor exists.

4.3 Genetic background in hetMNA neuroblastoma

HetMNA neuroblastomas are an exceptional subgroup of *MYCN*- amplified tumors given that MNA tumor cells often compose only the minority of cells in these tumors. The majority of tumor cells show no amplification. *MYCN*-amplified NB cells are not considered to proliferate slower than the other tumor cells. Therefore, we can assume that unamplified tumor cells emerged earlier than the *MYCN*-amplified ones giving rise to the different population sizes. Furthermore, we identified different amplicon compositions in the same NB tumor. Hence, we hypothesized that hetMNA NB tumors are prone to develop *MYCN* amplification and can do so independently in different tumor cells. To find support for this theory, we focused on chromosomal aberrations in the genomic background as potential triggers for MNA and looked for congruence in heterogeneous tumors of five different NB patients. We applied 250K SNP arrays in our investigation of a total of 13 tumor pieces.

Numerous chromosomes were mutually overrepresented in their entirety in all 13 tumor samples, which was expected since the tumors were at least near-triploid. Except in a near-hexaploid tumor, chromosome 19 appeared disomic in the other four tumors. To our knowledge, whole chromosome 19 underrepresentation has not been linked to tumorigenesis in cancer. Any relevance is difficult to imagine since this chromosome was disomic. A common segmental aberration, however, was not detectable at the resolution of the applied SNP arrays and can thus be excluded as a sole initiator of MNA. The fact that MNA occurs independently from a specific larger segmental aberration in heterogeneous tumors can already be concluded from the SNP array profiles of tumor pieces of two patients. While distinctive *MYCN* amplifications were present, SCAs were not detectable. A 1p-loss is often associated with MNA in homogeneously amplified NB, but MNA without any other segmental aberration has only been reported in very few cases in the literature. Albeit our results showed no commonality in large SCAs, segmental microaberrations or other mutations could still underlie MNA. Though, their investigation was not included in this project. Next-generation sequencing of the tumor DNA or of expressed genes could offer more detailed information whether minor alterations or expression differences play a role.

Nonetheless, our results indeed demonstrated the association of an immense variety of segmental aberrations with hetMNA, including losses of 1p, 11q, 12q, and 17p and segmental gains of 2p, 3p, and 6p in different tumor pieces of only three patients. The most interesting

combination of aberrations was revealed in the four pieces of the tumor of patient #4. While all four pieces showed 1p-losses in one of three chromosomes in cell populations of varying sizes, two distinct 1p breakpoints were detectable in two tumor pieces each. Further investigations of the breakpoints were not undertaken and their emergence is thus subject to speculations. The two breaks could have developed independently from one another. The occurrence of the first break of the smaller aberration at a rather instable site, which subsequently lead to second, more stable break and a larger segmental loss, would be a different explanation. The 1p-losses were detected in combination with either MNA, 3q gain, 11q-loss or no other SCA in the four respective tumor samples, which indicates the existence of at least four different tumor cell clones in the entire tumor. The presence of MNA and 11q-LOH in the same tumor is remarkable since a striking inverse relationship of the two alterations has been confirmed in various studies [12, 126, 127]. In this case, it can also be assumed that MNA and 11q-LOH tumor cells constitute different populations within this tumor. The tumor piece displaying MNA showed no sign of 11q-loss and vice versa. Confirmation by a clarifying I-FISH for the presence of any combined alterations within the single tumor pieces has not yet been obtained. Therefore, it cannot be said whether the aberrations occurred in the same or in distinctive cell population in the four tumor pieces. Assuming that even more tumor cell clones are comprised in the entire tumor is reasonable. Dissection of the different tumor cell types and comparison of their genomic profile would allow a prediction on clonality and could potentially reveal a chronology of aberration emergence in the different cell populations.

The case of patient #5 is a good example for the importance of a good tumor workup supporting the obligatory application of I-FISH in NB diagnostics. While the sample of the initial tumor showed no MNA with SNP array analysis, *MYCN* I-FISH identified a few tumor cells with amplification in touch preparations. The tumor piece removed during therapy showed a very prominent amplification of *MYCN* on the SNP array. Apparently, the primary tumor was resected incompletely. The remainder with a majority of MNA cells was either unresected or the sparse *MYCN* amplified cells gained a natural proliferative advantage over the other tumor cells or were selected for by the applied therapy. A new origination of the neuroblastoma is unlikely since both tumors showed almost identical numerical aberrations (data not shown).

The disclosed heterogeneity of the investigated hetMNA tumors argues for the resection and investigation of more, separated tumor pieces for a better identification of individual tumor cell clones. The effect on risk stratification and survival of coexisting NB clones and their potential cooperation has been largely unexplored to our knowledge and demands a more detailed investigation.

4.4 Genetic instability in neuroblastoma

MYCN amplification is considered to emerge rather late in the tumorigenesis of neuroblastoma and is thus not present in every tumor [123]. MNA is not required for NB development, but associates with aggressive behavior in advanced diseases and worse prognosis [114]. An underlying chronological order of genetic events leading to NB formation and in particular to MNA is yet to be identified. Earlier, we have reported that a common segmental aberration does not correlate with *MYCN* amplification in hetMNA tumors. A common ground, however, exists during the formation of MNA in all tumors. Genomic instability-entailed DNA double strand-breaks lie at the heart of the formation of both extrachromosomal double minutes and chromosomal homogeneously staining regions, the two cytogenetic manifestations of MNA in neuroblastoma [29]. Chromosomal breakage is necessary to initiate both the breakage-fusion-bridge cycle and the episome model. Both processes are considered to result in both cytogenetic manifestations of the *MYCN* amplicon [32, 37, 128]. Hence, we investigated genomic instability and DSB occurrence as a potential trigger for *MYCN* amplification and correlated γ H2AX immunostaining to subsequent *MYCN* I-FISH.

Our experiments permit the conclusion that unrepaired DNA double strand breaks, as visualized by γ H2AX immunostaining, are detectable in tumor cells independently from *MYCN* amplification in neuroblastoma. Furthermore, *MYCN* amplification is present without a correlating γ H2AX staining in tumor cells of heterogeneous and homogeneous MNA tumors. The overall staining was heterogeneous in pattern and mostly diffuse with only a few foci in the nuclei of all tested tumor samples including the homogeneous references. The strongest staining was detected in neuroblastomas featuring a combination of MNA and

segmental aberrations. The difference between tumors with NCA-only and those with segmental aberrations is less prominent and needs to be further distinguished with more tumor samples. Genetically different hetMNA neuroblastoma were also different in their γ H2AX staining pattern and can thus far not be assigned to any of the three categories of homogeneous neuroblastoma. Interestingly, the hetMNA tumor without SCAs showed a stronger staining pattern than the one with SCAs.

The presence of MNA cells which showed dmin-typical *MYCN* FISH spots without γ H2AX staining in the amplified tumor subgroups suggests that episomal *MYCN* amplification leaves no unrepaired DSBs behind when DNA damage repair is not compromised otherwise. Incomplete repair of the damage in γ H2AX positive cells could potentially elicit a response towards senescence or even apoptosis, which is a typical signature of aggressively proliferating MNA tumor cells [129]. Interpreting MNA and γ H2AX correlation events in terms of the state of the affected cell is therefore more complicated. Dual-positivity could generally indicate a high basic level of DSB presence. Alternatively, the already established *MYCN* amplification could lead to oncogene-induced DSB formation. For an accurate interpretation, we also need to take into account that other cellular processes lead to phosphorylation of γ H2AX as well. Apoptotic cells also stain strongly for γ H2AX and usually show a unique DAPI staining in the advanced apoptotic nuclei (data not shown). Early stages are more difficult to identify by DAPI alone but an affected cell undergoing the initial steps of DNA fragmentation with irreparable DSBs would still stain positive. Additionally, *MYCN* overexpression was shown to induce apoptosis in cell lines [130]. An apoptosis assay might help to discriminate these cells from viable γ H2AX-positive tumor cells. Phosphorylation of H2AX has furthermore been reported in association with eroded telomeres [131, 132] and to occur independently from DSBs and DNA damage signaling in a cell-cycle dependent manner [133]. Both causations need to be excluded by further experiments in order to implicate genomic instability in *MYCN* amplification.

A neuroblastoma without MNA presenting a MLPA-detected 11q-loss was also included in our investigation. The deleted region included the 11q23.2-q23.3 segment which is known to contain the *H2AFX* gene. Carén *et al.* recently published their results linking deletion of this specific region to a reduced *H2AFX* expression and chromosomal instability in high-risk NB [12]. Our results show γ H2AX-positivity in a few tumor cells. Apparently, residual *H2AFX* expression still leads to DSB detection by γ H2AX and supposedly to DNA damage response.

Correlation with 11q-deletion was, however, not examined specifically by I-FISH in the γ H2AX-positive tumor cells.

Although our study needs to be enlarged including more heterogeneous and homogenous NB tumors to support our findings, we can already conclude that *MYCN* amplification in homogeneous neuroblastoma coincides with the strongest γ H2AX detection of all genetic subgroups. However, we cannot tie genomic instability indisputably to the accrument of *MYCN* amplification in hetMNA tumors with γ H2AX immunohistochemical staining alone. Conducting the aforementioned experiments could aid in obtaining a clearer picture. Furthermore, working with cryosections of patient material gives a valuable, *in vivo* overview of the DSB presence in tumors of the different NB subcategories. However, cryosections may not be best suited to resolve the question whether genomic instability or the *MYCN* oncogene is responsible for the induction of DNA double strand breaks in amplified tumor cells. Nonetheless, combining γ H2AX detection with other genetic or cellular markers has the potential to shed light on the surrounding circumstances of DSB induction. Additionally, oncogene- versus genomic instability- induced DSB formation could be investigated by comparing the γ H2AX profile of *MYCN*-overexpressing to *MYCN*- amplified NB cell lines. Another interesting experiment would involve investigating the potential of *MYCN*-amplified cells to elicit a bystander response on non-amplified tumor cells. A medium transfer experiment of irradiated human skin fibroblasts resulted in the relay of the DSB formation and response to non-irradiated cells cultured independently with the medium of the irradiated cells [134]. The secreted soluble factors which initiated DSB formation in non-irradiated cells were assumed to contain signaling molecules related to ROS, such as nitric oxide. Whether *MYCN*-amplified NB cells have a similar influence on surrounding non-amplified tumor cells has never been examined and could help to explain the induction of DSBs in these cells, which were frequently found to be strongly γ H2AX positive in close proximity to MNA cells in hetMNA tumors.

5 List of Abbreviations

BFB	break-fusion-bridge
bHLH	basic helix-loop-helix
CCRI	Children's Cancer Research Institute
CIN	chromosomal instability
Cy3	cyanine 3
D.T.	during therapy
DAPI	4',6-diamidino-2-phenylindole
DIG	digoxigenin
dmin	double-minutes
dNTP	deoxyribonucleotide
DSB	double-strand break
FITC	Fluorescein isothiocyanate
FOV	field of vision
hetMNA	heterogeneous <i>MYCN</i> amplification
hsr	homologous staining regions
HU	hydroxyurea
I-FISH	Interphase fluorescent <i>in situ</i> hybridization
INRG	International Neuroblastoma Risk Grouping
LOH	loss of heterozygosity
MIN	microsatellite instability
MLPA	Multiplex ligation-dependent probe amplification
MNA	<i>MYCN</i> amplification
NCA	numeric chromosomal aberration
PCR	Polymerase chain reaction
PIN	point mutation instability
PNET	peripheral neuroectodermal tumors
SCA	segmental chromosomal aberration
SCLC	small cell lung cancer
SNP	single nucleotide polymorphism
T-ALL	T- cell acute lymphoblastic leukemia

6 List of Figures

- Figure 1: Coamplification in the *MYCN* amplicon is distance-related [44]. (A) Coamplification frequencies of the seven investigated genes on chromosome 2p24-25 in 98 primary NB tumors. (B) Physical distance of the seven investigated genes in relation to *MYCN*, based on current BLAT assignment information [42]..... 12
- Figure 2: Histopathological and interphase FISH stainings of tumor sections. All sections were cut at 5µm in a cryostat. (A) Histopathological HE staining of fibrous stroma-poor area of a NB section. (B) HE staining of a stroma-rich area of a tumor section. (C) FITC-, Cy3- and merged image with DAPI background of an area in a heterogeneous NB section. *MYCN* is green, D2Z red and DNA blue. White arrows mark disomic cells, red arrows mark tumor cell trisomic for chromosome 2 and the red arrow head a *MYCN* amplified cell. White bars, 10µm. 32
- Figure 3: Comparison of MLPA and FISH results on *MYCN* amplicon detection and composition. Examination of a tumor DNA from patient #4 is done by MLPA (A) and SNP array analysis (B). The red rectangle in the MLPA readout of chromosome 2 marks the two *MYCN* probes. In the SNP array data, *MYCN* amplification is marked by the red arrow in the single-chromosome view of chromosome 2. The blue line illustrates the average copy number of both alleles; red (large) and green (small) lines depict allele based analyses. Chromosomes are represented by their cytoband information. Interphase fluorescent *in situ* hybridization (FISH) validates of MNA with *MYCN* (green) and D2Z (red) probes (C). Composition of the *MYCN* amplicon is confirmed with probes for *MYCN* (green) and *DDX1* (red) (D). White arrows point out good examples of *MYCN*-amplified cells. White bar, 10µm..... 35
- Figure 4: MLPA and SNP array of a heterogeneous tumor do not always correlate with *MYCN* I-FISH results. Examination of a patient's tumor DNA is done by MLPA (A) and SNP array analysis (B). The black rectangle in the MLPA readout of chromosome 2 frames the probes often comprised in a *MYCN* amplicon. The SNP array data is displayed in the single-chromosome view of chromosome 2. The blue line illustrates the average copy number of both alleles; red (large) and green (small) lines depict allele based analyses. Chromosomes are represented by their cytoband information. Interphase fluorescent *in situ* hybridization (FISH) validates of MNA with *MYCN* (green) and D2Z (red) probes (C). Composition of the *MYCN* amplicon is examined with probes for *MYCN* (green) and *NAG* (red) (D). White arrows point out good examples of *MYCN*-amplified cells. White bar, 10µm..... 36
- Figure 5: Heterogeneity in size and composition of the *MYCN* amplicon in a hetMNA neuroblastoma. (A) MLPA data of chromosome 2 shown with a red rectangle marking the amplified genes. In the single-chromosome view of SNP array data on chromosome 2 is displayed (B). The large amplicon in marked by the black bar and the *MYCN*-only amplification by the red arrow. The blue line illustrates the average copy number of both alleles; red (large) and green (small) lines depict allele based analyses. Chromosomes are represented by their cytoband information. (C) I-FISH stainings with probes for *MYCN* (green) and *DDX1* (red) were applied to illustrate the heterogeneous amplicon structure. *DDX1*-coamplified tumor cells are marked by white arrows in the upper panel. A cell carrying the “*MYCN*-only” amplicon is pictured in the lower panel. White bars, 10µm... 38

Figure 6: All genome view of SNP array data provided an excellent overview of genomic aberrations in tumor samples. SNP array data from patient #1 is shown in the all-genome-view generated. The blue line illustrates the average copy number of both alleles; red (large) and green (small) lines depict allele based analyses. Chromosomes are represented by cytobands information. The red arrow points at the *MYCN*-location on chromosome 2, while black arrows mark chromosomal break points and asterisks other amplifications. For better visualization of segmental aberrations, gains are highlighted in transparent red and losses in transparent green. 40

Figure 7: One out of four tumor pieces from patient #2 showed a 17p- deletion. SNP array analysis was done on the four tumor pieces of patient #2 labeled A to D. Chromosome 17 is shown in the single-chromosome-view. The blue line illustrates the average copy number of both alleles; red (large) and green (small) lines depict allele based analyses. The chromosome is represented by the cytoband information. For better visualization of the 17p segmental aberrations, the loss is highlighted in transparent green and the black arrow marks the break point. 42

Figure 8: MNA heterogeneity was detected in the two tumor pieces of patient #3. Pieces A and B were screened for chromosomal aberrations with SNP arrays. The single chromosome views are shown in the black boxes for chromosome 2. The *MYCN* amplicon is marked by a black bar and the location of *MYCN* gene indicated by the red arrow. The blue line illustrates the average copy number of both alleles; red (large) and green (small) lines depict allele based analyses. The chromosome is represented by its cytoband information. 43

Figure 9: Four tumor pieces of patient #4 revealed extensive genetic heterogeneity. SNP array data of patient #4 is shown in an overview of selected single-chromosome-views generated with the CNAG 3.0 software. Chromosomes 1, 2, 3 and 11 were selected because of heterogeneous genetic aberrations. The blue line illustrates the average copy number of both alleles; red (large) and green (small) lines depict allele based analyses. Chromosomes are represented by their cytoband information. The red arrow points out the genomic *MYCN* location, while black arrows mark chromosomal break points. For better visualization of segmental aberrations, gains are highlighted in transparent red and losses in transparent green. 45

Figure 10: Heterogeneity of MNA was detectable in the initial tumor and in the resected tumor during treatment. The two pieces of patient #5 were screened for chromosomal aberrations with SNP arrays. Single-chromosome-views are shown for chromosome 2, 17, and 20. The *MYCN* amplicon is indicated by a red arrow. The amplification on chromosome 17 is marked with a blue arrow and the deletion on chromosome 20 with a green arrow. The blue line illustrates the average copy number of both alleles; red (large) and green (small) lines depict allele based analyses. The chromosome is represented by its cytoband..... 46

Figure 11: Heterogeneous tumors show no common segmental aberration. Affymetrix GeneChip® Human Mapping 250K Nsp Arrays were used to investigate the genetic background of hetMNA NB. The different tumor samples were compared to one another. The light pink color marks entire overrepresented chromosomes, light red depicts gained segmental aberrations and dark green lost segmental aberrations. The dark red bands illustrate amplifications and green bands deletions. The bands for the *MYCN* amplicon and other single-gene aberrations are slightly broadened for better visualization and do not resemble the actual size of the amplicon. Since the analysis of the array data is based on a

diploid karyotype, white color indicates disomic chromosomes. * The tumor of patient #1 showed strong heterogeneity in the *MYCN* I-FISH results. ** The two compared tumor pieces of patient #5 were primary and during-therapy. Pat. # patient number; Tu. # tumor number: In initial: D.T. during therapy 47

Figure 12: *MYCN* amplification only partially correlates with the occurrence of DNA double strand breaks in hetMNA neuroblastoma. Images show combined stainings of FITC-labeled *MYCN* I-FISH (left column) on Cy3-labeled γ H2AX prestained cryosections (middle column) of hetMNA tumor pieces. Merged images of FITC, Cy3 and DAPI are depicted in the right column. Stainings of two tumor pieces of the same hetMNA neuroblastoma with NCA are displayed; one piece with a very low percentage or no MNA cells (A), the other with a high percentage of MNA cells (B). Two pieces of a hetMNA tumor with SCA are depicted in the lower two rows, one with no detectable MNA cells (C) the other with large areas of amplified cells (D). White arrows point at tumor cells with little or no γ H2AX staining, red arrows at tumor cells with γ H2AX staining, the arrow heads at double-positives, and the green arrow at a disomic cell of unknown cell type. White bar, 10 μ m. 49

Figure 13: γ H2AX staining pattern is heterogeneous in different hetMNA neuroblastoma and compares weakly to homogeneous tumors. Overview images and the detailed images in the panel below are always from the same tumor. Overviews are stained for γ H2AX and counterstained with DAPI. In the panel of the detailed images, *MYCN*- FISH is green (left image), γ H2AX immunostaining is red (middle image). Merged images (right image) are counterstained with DAPI (blue). Correlated stainings are displayed for γ H2AX and *MYCN* amplification in a hetMNA tumor with NCA (A) and a hetMNA tumor carrying SCAs (B). References of *MYCN* I-FISH and γ H2AX immunostaining on sections of homogeneous NBs with NCA without MNA (C), SCAs without MNA (D) and SCAs with classic MNA (E) are given below. Red arrows denote positive and white arrows negative tumor cells for γ H2AX staining. Red arrow heads identify double-positive cells. The green arrow marks a γ H2AX positive cell of unknown cell type. White bars, 10 μ m. 51

Figure 14: “Classic” MNA neuroblastoma display areas without and with strong γ H2AX immunostaining. Images show combined stainings of FITC-labeled *MYCN* I-FISH (left column) on Cy3-labeled γ H2AX prestained cryosections (middle column) of MNA tumor pieces. Merged images of FITC, Cy3 and DAPI are depicted in the right column. Red arrows mark tumor cells with strong γ H2AX positivity. Images were taken at 40-fold magnification with fixed integration times. White bar, 10 μ m. 52

Figure 15: Neuroblastoma with 11q-loss shows substantial γ H2AX staining. MLPA displays prominent 11q deletion including the *H2AFX* gene locus (A). The detailed images (B) in the panel below and part of section overview (C) are from the same tumor. *MYCN*- FISH is green, γ H2AX immunostaining is red and DNA is blue for all images. Images were taken at 40-fold magnification with fixed integration times and stitched together for the overview. Black rectangle marks the lost segment on chromosome 11. White arrows mark examples of γ H2AX negative tumor cells and green arrows positive cell of unknown cell type. White bar, 10 μ m. 53

7 List of Tables

Table 1: Clinical and therapy data of the five patients selected for genetic analysis..... 20

Table 2: MLPA reaction mixes. Depending on the number of DNA samples the reaction mixes were done as master mixes. All reagents were obtained from MRC Holland except for aqua dest. and HiDi-formamide (Applied Biosystems, Darmstadt, Germany; Cat. No. P/N4311320C)..... 27

8 Reference

1. Norman J Lacayo, M. and M. Neyssa Marina. *Neuroblastoma*. 2007 14.11.2007 [cited 2009 25.02.]; Available from: <http://emedicine.medscape.com/article/988284-overview>.
2. Brodeur, G.M., et al., *Revisions of the international criteria for neuroblastoma diagnosis, staging and response to treatment*. Prog Clin Biol Res, 1994. **385**: p. 363-9.
3. Ambros, P.F., et al., *Regression and progression in neuroblastoma. Does genetics predict tumour behaviour?* Eur J Cancer, 1995. **31A**(4): p. 510-5.
4. Ambros, I.M., et al., *Role of ploidy, chromosome 1p, and Schwann cells in the maturation of neuroblastoma*. N Engl J Med, 1996. **334**(23): p. 1505-11.
5. Gisselsson, D., et al., *Distinct evolutionary mechanisms for genomic imbalances in high-risk and low-risk neuroblastomas*. J Carcinog, 2007. **6**: p. 15.
6. Spitz, R., et al., *Oligonucleotide array-based comparative genomic hybridization (aCGH) of 90 neuroblastomas reveals aberration patterns closely associated with relapse pattern and outcome*. Genes Chromosomes Cancer, 2006. **45**(12): p. 1130-42.
7. Kaneko, Y., et al., *Different karyotypic patterns in early and advanced stage neuroblastomas*. Cancer Res, 1987. **47**(1): p. 311-8.
8. Spitz, R., et al., *Favorable outcome of triploid neuroblastomas: a contribution to the special oncogenesis of neuroblastoma*. Cancer Genet Cytogenet, 2006. **167**(1): p. 51-6.
9. Seeger, R.C., et al., *Association of multiple copies of the N-myc oncogene with rapid progression of neuroblastomas*. N Engl J Med, 1985. **313**(18): p. 1111-6.
10. Attiyeh, E.F., et al., *Chromosome 1p and 11q deletions and outcome in neuroblastoma*. N Engl J Med, 2005. **353**(21): p. 2243-53.
11. Bown, N., et al., *Gain of chromosome arm 17q and adverse outcome in patients with neuroblastoma*. N Engl J Med, 1999. **340**(25): p. 1954-61.
12. Caren, H., et al., *High-risk neuroblastoma tumors with 11q-deletion display a poor prognostic, chromosome instability phenotype with later onset*. Proc Natl Acad Sci U S A. **107**(9): p. 4323-8.
13. Vandesompele, J., et al., *Genetic heterogeneity of neuroblastoma studied by comparative genomic hybridization*. Genes Chromosomes Cancer, 1998. **23**(2): p. 141-52.
14. Schleiermacher, G., et al., *Accumulation of segmental alterations determines progression in neuroblastoma*. Journal of Clinical Oncology, 2010.
15. American Cancer Society, I. *Detailed Guide: Neuroblastoma What Are the Risk Factors for Neuroblastoma?* 22.10.2008 [cited 2009 26.02].
16. Corvi, R., et al., *MYCN is retained in single copy at chromosome 2 band p23-24 during amplification in human neuroblastoma cells*. Proc Natl Acad Sci U S A, 1994. **91**(12): p. 5523-7.
17. Schwab, M., et al., *Amplified DNA with limited homology to myc cellular oncogene is shared by human neuroblastoma cell lines and a neuroblastoma tumour*. Nature, 1983. **305**(5931): p. 245-8.
18. Kohl, N.E., et al., *Transposition and amplification of oncogene-related sequences in human neuroblastomas*. Cell, 1983. **35**(2 Pt 1): p. 359-67.
19. Squire, J., et al., *Tumour induction by the retinoblastoma mutation is independent of N-myc expression*. Nature, 1986. **322**(6079): p. 555-7.

20. Zimmerman, K.A., et al., *Differential expression of myc family genes during murine development*. Nature, 1986. **319**(6056): p. 780-3.
21. Schwab, M., R. Corvi, and L.C. Amler, *N-MYC oncogene amplification: a consequence of genomic instability in human neuroblastoma*. The Neuroscientist 1995. **1**: p. 277-285.
22. Nau, M.M., et al., *Human small-cell lung cancers show amplification and expression of the N-myc gene*. Proc Natl Acad Sci U S A, 1986. **83**(4): p. 1092-6.
23. Lee, W.H., A.L. Murphree, and W.F. Benedict, *Expression and amplification of the N-myc gene in primary retinoblastoma*. Nature, 1984. **309**(5967): p. 458-60.
24. Collins, V.P., *Amplified genes in human gliomas*. Semin Cancer Biol, 1993. **4**(1): p. 27-32.
25. Rouah, E., et al., *N-myc amplification and neuronal differentiation in human primitive neuroectodermal tumors of the central nervous system*. Cancer Res, 1989. **49**(7): p. 1797-801.
26. Stanton, L.W., M. Schwab, and J.M. Bishop, *Nucleotide sequence of the human N-myc gene*. Proc Natl Acad Sci U S A, 1986. **83**(6): p. 1772-6.
27. Ibson, J.M. and P.H. Rabbitts, *Sequence of a germ-line N-myc gene and amplification as a mechanism of activation*. Oncogene, 1988. **2**(4): p. 399-402.
28. Smith, K.A., et al., *Distinctive chromosomal structures are formed very early in the amplification of CAD genes in Syrian hamster cells*. Cell, 1990. **63**(6): p. 1219-27.
29. Debatisse, M., et al., *Gene amplification mechanisms: the role of fragile sites*. Recent Results Cancer Res, 1998. **154**: p. 216-26.
30. Coquelle, A., et al., *Expression of fragile sites triggers intrachromosomal mammalian gene amplification and sets boundaries to early amplicons*. Cell, 1997. **89**(2): p. 215-25.
31. Shimizu, N., et al., *When, where and how the bridge breaks: anaphase bridge breakage plays a crucial role in gene amplification and HSR generation*. Exp Cell Res, 2005. **302**(2): p. 233-43.
32. Vukovic, B., et al., *Correlating breakage-fusion-bridge events with the overall chromosomal instability and in vitro karyotype evolution in prostate cancer*. Cytogenet Genome Res, 2007. **116**(1-2): p. 1-11.
33. Selvarajah, S., et al., *The breakage-fusion-bridge (BFB) cycle as a mechanism for generating genetic heterogeneity in osteosarcoma*. Chromosoma, 2006. **115**(6): p. 459-67.
34. Reshmi, S.C., et al., *Inverted duplication pattern in anaphase bridges confirms the breakage-fusion-bridge (BFB) cycle model for 11q13 amplification*. Cytogenet Genome Res, 2007. **116**(1-2): p. 46-52.
35. Carroll, S.M., et al., *Double minute chromosomes can be produced from precursors derived from a chromosomal deletion*. Mol Cell Biol, 1988. **8**(4): p. 1525-33.
36. Wahl, G.M., *The importance of circular DNA in mammalian gene amplification*. Cancer Res, 1989. **49**(6): p. 1333-40.
37. Von Hoff, D.D., *New mechanisms of gene amplification in drug resistance (the episome model)*. Cancer Treat Res, 1991. **57**: p. 1-11.
38. Storlazzi, C.T., et al., *MYC-containing double minutes in hematologic malignancies: evidence in favor of the episome model and exclusion of MYC as the target gene*. Hum Mol Genet, 2006. **15**(6): p. 933-42.

39. Yoshimoto, M., et al., *MYCN gene amplification. Identification of cell populations containing double minutes and homogeneously staining regions in neuroblastoma tumors*. Am J Pathol, 1999. **155**(5): p. 1439-43.
40. Storlazzi, C.T., et al., *Origin and structure of MYCN-containing double minutes (dmin) and homogeneously staining regions (hsr) in solid tumors*. Genome Research, 2010.
41. Hahn, P.J., *Molecular biology of double-minute chromosomes*. Bioessays, 1993. **15**(7): p. 477-84.
42. Reiter, J.L. and G.M. Brodeur, *High-resolution mapping of a 130-kb core region of the MYCN amplicon in neuroblastomas*. Genomics, 1996. **32**(1): p. 97-103.
43. Hiemstra, J.L., S.S. Schneider, and G.M. Brodeur, *High-resolution mapping of the N-myc amplicon core domain in neuroblastomas*. Prog Clin Biol Res, 1994. **385**: p. 51-7.
44. Weber, A., et al., *Coamplification of DDX1 correlates with an improved survival probability in children with MYCN-amplified human neuroblastoma*. J Clin Oncol, 2004. **22**(13): p. 2681-90.
45. George, R.E., et al., *Analysis of candidate gene co-amplification with MYCN in neuroblastoma*. Eur J Cancer, 1997. **33**(12): p. 2037-42.
46. Chen, B., S.C. Jhanwar, and M. Ladanyi, *Rearrangement in the coding region of the MYCN gene in a subset of amplicons in a case of neuroblastoma with MYCN amplification*. Diagn Mol Pathol, 2001. **10**(2): p. 100-4.
47. Lutz, W. and M. Schwab, *In vivo regulation of single copy and amplified N-myc in human neuroblastoma cells*. Oncogene, 1997. **15**(3): p. 303-15.
48. Theissen, J., et al., *Heterogeneity of the MYCN oncogene in neuroblastoma*. Clin Cancer Res, 2009. **15**(6): p. 2085-90.
49. Kushima, M., et al., *Heterogeneity and progression of renal cell carcinomas as revealed by DNA cytofluorometry and the significance of the presence of polyploid cells*. Urol Res, 1995. **23**(6): p. 381-6.
50. Sayagues, J.M., et al., *Incidence of numerical chromosome aberrations in meningioma tumors as revealed by fluorescence in situ hybridization using 10 chromosome-specific probes*. Cytometry, 2002. **50**(3): p. 153-9.
51. Okada, S., et al., *Intratumoral DNA heterogeneity of small hepatocellular carcinoma*. Cancer, 1995. **75**(2): p. 444-50.
52. Lonn, U., et al., *Intratumoral heterogeneity for amplified genes in human breast carcinoma*. Int J Cancer, 1994. **58**(1): p. 40-5.
53. Kerbl, R., et al., *Neuroblastoma with focal MYCN amplification and bone marrow infiltration: a staging and treatment dilemma*. Med Pediatr Oncol, 2002. **38**(2): p. 109-11.
54. Lorenzana, A.N., et al., *Heterogeneity of MYCN amplification in a child with stroma-rich neuroblastoma (ganglioneuroblastoma)*. Pediatr Pathol Lab Med, 1997. **17**(6): p. 875-83.
55. Noguera, R., et al., *MYCN gain and MYCN amplification in a stage 4S neuroblastoma*. Cancer Genet Cytogenet, 2003. **140**(2): p. 157-61.
56. Negrini, S., V.G. Gorgoulis, and T.D. Halazonetis, *Genomic instability--an evolving hallmark of cancer*. Nat Rev Mol Cell Biol. **11**(3): p. 220-8.
57. Fishel, R., et al., *The human mutator gene homolog MSH2 and its association with hereditary nonpolyposis colon cancer*. Cell, 1993. **75**(5): p. 1027-38.
58. Leach, F.S., et al., *Mutations of a mutS homolog in hereditary nonpolyposis colorectal cancer*. Cell, 1993. **75**(6): p. 1215-25.

59. Al-Tassan, N., et al., *Inherited variants of MYH associated with somatic G:C-->T:A mutations in colorectal tumors*. Nat Genet, 2002. **30**(2): p. 227-32.
60. Bielas, J.H., et al., *Human cancers express a mutator phenotype*. Proc Natl Acad Sci U S A, 2006. **103**(48): p. 18238-42.
61. Loeb, L.A., K.R. Loeb, and J.P. Anderson, *Multiple mutations and cancer*. Proc Natl Acad Sci U S A, 2003. **100**(3): p. 776-81.
62. Eshleman, J.R., et al., *Increased mutation rate at the hprt locus accompanies microsatellite instability in colon cancer*. Oncogene, 1995. **10**(1): p. 33-7.
63. Malkhosyan, S., et al., *Frameshift mutator mutations*. Nature, 1996. **382**(6591): p. 499-500.
64. Terrados, G., et al., *Characterization of a natural mutator variant of human DNA polymerase lambda which promotes chromosomal instability by compromising NHEJ*. PLoS One, 2009. **4**(10): p. e7290.
65. Kinzler, K.W. and B. Vogelstein, *Cancer-susceptibility genes. Gatekeepers and caretakers*. Nature, 1997. **386**(6627): p. 761, 763.
66. Shen, C.Y., et al., *Genome-wide search for loss of heterozygosity using laser capture microdissected tissue of breast carcinoma: an implication for mutator phenotype and breast cancer pathogenesis*. Cancer Res, 2000. **60**(14): p. 3884-92.
67. Cahill, D.P., et al., *Mutations of mitotic checkpoint genes in human cancers*. Nature, 1998. **392**(6673): p. 300-3.
68. Cahill, D.P., et al., *Characterization of MAD2B and other mitotic spindle checkpoint genes*. Genomics, 1999. **58**(2): p. 181-7.
69. Wang, Z., et al., *Three classes of genes mutated in colorectal cancers with chromosomal instability*. Cancer Res, 2004. **64**(9): p. 2998-3001.
70. Halazonetis, T.D., V.G. Gorgoulis, and J. Bartek, *An oncogene-induced DNA damage model for cancer development*. Science, 2008. **319**(5868): p. 1352-5.
71. Casper, A.M., et al., *ATR regulates fragile site stability*. Cell, 2002. **111**(6): p. 779-89.
72. Arlt, M.F., A.M. Casper, and T.W. Glover, *Common fragile sites*. Cytogenet Genome Res, 2003. **100**(1-4): p. 92-100.
73. Durkin, S.G. and T.W. Glover, *Chromosome fragile sites*. Annu Rev Genet, 2007. **41**: p. 169-92.
74. Gorgoulis, V.G., et al., *Activation of the DNA damage checkpoint and genomic instability in human precancerous lesions*. Nature, 2005. **434**(7035): p. 907-13.
75. Bartkova, J., et al., *DNA damage response as a candidate anti-cancer barrier in early human tumorigenesis*. Nature, 2005. **434**(7035): p. 864-70.
76. Di Micco, R., et al., *Oncogene-induced senescence is a DNA damage response triggered by DNA hyper-replication*. Nature, 2006. **444**(7119): p. 638-42.
77. Denko, N.C., et al., *The human Ha-ras oncogene induces genomic instability in murine fibroblasts within one cell cycle*. Proc Natl Acad Sci U S A, 1994. **91**(11): p. 5124-8.
78. Felsher, D.W. and J.M. Bishop, *Transient excess of MYC activity can elicit genomic instability and tumorigenesis*. Proc Natl Acad Sci U S A, 1999. **96**(7): p. 3940-4.
79. Bartkova, J., et al., *Oncogene-induced senescence is part of the tumorigenesis barrier imposed by DNA damage checkpoints*. Nature, 2006. **444**(7119): p. 633-7.
80. Kastan, M.B. and J. Bartek, *Cell-cycle checkpoints and cancer*. Nature, 2004. **432**(7015): p. 316-23.
81. Hollstein, M., et al., *p53 mutations in human cancers*. Science, 1991. **253**(5015): p. 49-53.

82. Stiff, T., et al., *ATR-dependent phosphorylation and activation of ATM in response to UV treatment or replication fork stalling*. EMBO J, 2006. **25**(24): p. 5775-82.
83. Stiff, T., et al., *ATM and DNA-PK function redundantly to phosphorylate H2AX after exposure to ionizing radiation*. Cancer Res, 2004. **64**(7): p. 2390-6.
84. Takahashi, A. and T. Ohnishi, *Does gammaH2AX foci formation depend on the presence of DNA double strand breaks?* Cancer Lett, 2005. **229**(2): p. 171-9.
85. Rogakou, E.P., et al., *Megabase chromatin domains involved in DNA double-strand breaks in vivo*. J Cell Biol, 1999. **146**(5): p. 905-16.
86. Stucki, M. and S.P. Jackson, *gammaH2AX and MDC1: anchoring the DNA-damage-response machinery to broken chromosomes*. DNA Repair (Amst), 2006. **5**(5): p. 534-43.
87. Rappold, I., et al., *Tumor suppressor p53 binding protein 1 (53BP1) is involved in DNA damage-signaling pathways*. J Cell Biol, 2001. **153**(3): p. 613-20.
88. van Attikum, H. and S.M. Gasser, *ATP-dependent chromatin remodeling and DNA double-strand break repair*. Cell Cycle, 2005. **4**(8): p. 1011-4.
89. Chaplet, M., et al., *BRIT1/MCPH1: a guardian of genome and an enemy of tumors*. Cell Cycle, 2006. **5**(22): p. 2579-83.
90. Chaturvedi, P., et al., *Mammalian Chk2 is a downstream effector of the ATM-dependent DNA damage checkpoint pathway*. Oncogene, 1999. **18**(28): p. 4047-54.
91. Bartek, J. and J. Lukas, *Chk1 and Chk2 kinases in checkpoint control and cancer*. Cancer Cell, 2003. **3**(5): p. 421-9.
92. Alderton, G.K., et al., *Regulation of mitotic entry by microcephalin and its overlap with ATR signalling*. Nat Cell Biol, 2006. **8**(7): p. 725-33.
93. Sedelnikova, O.A., et al., *Quantitative detection of (125)IdU-induced DNA double-strand breaks with gamma-H2AX antibody*. Radiat Res, 2002. **158**(4): p. 486-92.
94. Rogakou, E.P., et al., *DNA double-stranded breaks induce histone H2AX phosphorylation on serine 139*. J Biol Chem, 1998. **273**(10): p. 5858-68.
95. Bassing, C.H., et al., *Histone H2AX: a dosage-dependent suppressor of oncogenic translocations and tumors*. Cell, 2003. **114**(3): p. 359-70.
96. Thirman, M.J., et al., *Rearrangement of the MLL gene in acute lymphoblastic and acute myeloid leukemias with 11q23 chromosomal translocations*. N Engl J Med, 1993. **329**(13): p. 909-14.
97. Parikh, R.A., et al., *Loss of distal 11q is associated with DNA repair deficiency and reduced sensitivity to ionizing radiation in head and neck squamous cell carcinoma*. Genes Chromosomes Cancer, 2007. **46**(8): p. 761-75.
98. Novik, K.L., et al., *Genetic variation in H2AFX contributes to risk of non-Hodgkin lymphoma*. Cancer Epidemiol Biomarkers Prev, 2007. **16**(6): p. 1098-106.
99. Srivastava, N., et al., *Copy number alterations of the H2AFX gene in sporadic breast cancer patients*. Cancer Genet Cytogenet, 2008. **180**(2): p. 121-8.
100. Celeste, A., et al., *H2AX haploinsufficiency modifies genomic stability and tumor susceptibility*. Cell, 2003. **114**(3): p. 371-83.
101. Bonner, W.M., et al., *GammaH2AX and cancer*. Nat Rev Cancer, 2008. **8**(12): p. 957-67.
102. Klaunig, J.E. and L.M. Kamendulis, *The role of oxidative stress in carcinogenesis*. Annu Rev Pharmacol Toxicol, 2004. **44**: p. 239-67.
103. Hussain, S.P., L.J. Hofseth, and C.C. Harris, *Radical causes of cancer*. Nat Rev Cancer, 2003. **3**(4): p. 276-85.

104. Tanaka, T., et al., *Constitutive histone H2AX phosphorylation and ATM activation, the reporters of DNA damage by endogenous oxidants*. Cell Cycle, 2006. **5**(17): p. 1940-5.
105. Szekeres, T., M. Fritzer-Szekeres, and H.L. Elford, *The enzyme ribonucleotide reductase: target for antitumor and anti-HIV therapy*. Crit Rev Clin Lab Sci, 1997. **34**(6): p. 503-28.
106. Pourquier, P. and Y. Pommier, *Topoisomerase I-mediated DNA damage*. Adv Cancer Res, 2001. **80**: p. 189-216.
107. Fortune, J.M. and N. Osheroff, *Topoisomerase II as a target for anticancer drugs: when enzymes stop being nice*. Prog Nucleic Acid Res Mol Biol, 2000. **64**: p. 221-53.
108. Takai, H., A. Smogorzewska, and T. de Lange, *DNA damage foci at dysfunctional telomeres*. Curr Biol, 2003. **13**(17): p. 1549-56.
109. d'Adda di Fagagna, F., *Living on a break: cellular senescence as a DNA-damage response*. Nat Rev Cancer, 2008. **8**(7): p. 512-22.
110. Tweddle, D.A., et al., *Evidence for the development of p53 mutations after cytotoxic therapy in a neuroblastoma cell line*. Cancer Res, 2001. **61**(1): p. 8-13.
111. Carr, J., et al., *Increased frequency of aberrations in the p53/MDM2/p14(ARF) pathway in neuroblastoma cell lines established at relapse*. Cancer Res, 2006. **66**(4): p. 2138-45.
112. Leslie, A., et al., *Mutations of APC, K-ras, and p53 are associated with specific chromosomal aberrations in colorectal adenocarcinomas*. Cancer Res, 2003. **63**(15): p. 4656-61.
113. Yaari, S., et al., *Disruption of cooperation between Ras and MycN in human neuroblastoma cells promotes growth arrest*. Clin Cancer Res, 2005. **11**(12): p. 4321-30.
114. Maris, J.M., et al., *Neuroblastoma*. Lancet, 2007. **369**(9579): p. 2106-20.
115. Ambros, P.F., et al., *International consensus for neuroblastoma molecular diagnostics: report from the International Neuroblastoma Risk Group (INRG) Biology Committee*. Br J Cancer, 2009. **100**(9): p. 1471-82.
116. Nannya, Y., et al., *A robust algorithm for copy number detection using high-density oligonucleotide single nucleotide polymorphism genotyping arrays*. Cancer Res, 2005. **65**(14): p. 6071-9.
117. Yamamoto, G., et al., *Highly sensitive method for genomewide detection of allelic composition in nonpaired, primary tumor specimens by use of affymetrix single-nucleotide-polymorphism genotyping microarrays*. Am J Hum Genet, 2007. **81**(1): p. 114-26.
118. Villamon, E., et al., *Comparison of different techniques for the detection of genetic risk-identifying chromosomal gains and losses in neuroblastoma*. Virchows Arch, 2008. **453**(1): p. 47-55.
119. Haupt, Y., et al., *Mdm2 promotes the rapid degradation of p53*. Nature, 1997. **387**(6630): p. 296-9.
120. Huguet, E.L., et al., *Differential expression of human Wnt genes 2, 3, 4, and 7B in human breast cell lines and normal and disease states of human breast tissue*. Cancer Res, 1994. **54**(10): p. 2615-21.
121. Albertson, D.G., *Gene amplification in cancer*. Trends Genet, 2006. **22**(8): p. 447-55.
122. Cohn, S.L., et al., *The International Neuroblastoma Risk Group (INRG) classification system: an INRG Task Force report*. J Clin Oncol, 2009. **27**(2): p. 289-97.

123. Brodeur, G.M., et al., *Amplification of N-myc in untreated human neuroblastomas correlates with advanced disease stage*. Science, 1984. **224**(4653): p. 1121-4.
124. Graux, C., et al., *Heterogeneous patterns of amplification of the NUP214-ABL1 fusion gene in T-cell acute lymphoblastic leukemia*. Leukemia, 2009. **23**(1): p. 125-33.
125. Weber, A., et al., *The coamplification pattern of the MYCN amplicon is an invariable attribute of most MYCN-amplified human neuroblastomas*. Clin Cancer Res, 2006. **12**(24): p. 7316-21.
126. Guo, C., et al., *Deletion of 11q23 is a frequent event in the evolution of MYCN single-copy high-risk neuroblastomas*. Med Pediatr Oncol, 2000. **35**(6): p. 544-6.
127. Spitz, R., et al., *Loss in chromosome 11q identifies tumors with increased risk for metastatic relapses in localized and 4S neuroblastoma*. Clin Cancer Res, 2006. **12**(11 Pt 1): p. 3368-73.
128. Shimizu, N., et al., *Amplification of plasmids containing a mammalian replication initiation region is mediated by controllable conflict between replication and transcription*. Cancer Res, 2003. **63**(17): p. 5281-90.
129. Shimada, H., et al., *The International Neuroblastoma Pathology Classification (the Shimada system)*. Cancer, 1999. **86**(2): p. 364-72.
130. Paffhausen, T., M. Schwab, and F. Westermann, *Targeted MYCN expression affects cytotoxic potential of chemotherapeutic drugs in neuroblastoma cells*. Cancer Lett, 2007. **250**(1): p. 17-24.
131. Olive, P.L., *Endogenous DNA breaks: gammaH2AX and the role of telomeres*. Aging (Albany NY), 2009. **1**(2): p. 154-6.
132. Nakamura, A.J., et al., *Telomere-dependent and telomere-independent origins of endogenous DNA damage in tumor cells*. Aging (Albany NY), 2009. **1**(2): p. 212-8.
133. Ichijima, Y., et al., *Phosphorylation of histone H2AX at M phase in human cells without DNA damage response*. Biochem Biophys Res Commun, 2005. **336**(3): p. 807-12.
134. Han, W., et al., *The early and initiation processes of radiation-induced bystander effects involved in the induction of DNA double strand breaks in non-irradiated cultures*. Br J Radiol, 2007. **80 Spec No 1**: p. S7-12.

Curriculum Vitae

Personal data

Name Dominik Bogen
Date and place of birth: 28.01.1985, Bonn- Bad Godesberg, Germany
Nationality: Germany

Education

09/1995 – 07/2001 Konrad Adenauer Gymnasium, Meckenheim, Germany
08/2001 – 07/2004 German School Washington, D.C., Potomac, M.D., USA
09/2004 – 06/2010 Studies of Molecular Biology, University of Vienna, Vienna, Austria

Research Experience

08/2005 Internship at the Laboratory of Immunology, University Clinic Bonn, Bonn, Germany
Laboratory of Jacob Nattermann, M.D. and Ulrich Spengler, M.D.
Investigation of surface receptors on human HIV/HCV infected T-lymphocytes
Nattermann, J. et al. Hepatitis C virus-induced secretion of inflammatory chemokines preferentially recruits NKG2A+CD8+ T cells. J Infect Dis 198, 213-7 (2008).

08/2006 Internship at the Laboratory of Immunology, University Clinic, Bonn, Germany
Laboratory of Jacob Nattermann, M.D. and Ulrich Spengler, M.D.

07/2007 – 08/2007 Internship at the Laboratory of Mammalian Genes and Development, National Institute of Child Health and Human Development, National Institutes of Health (NIH), Bethesda, MD, USA
Laboratory of Heiner Westphal, M.D.
Examination of the role of LDB1 in a valvular defect in *Mus Musculus*

09/2008 – 10/2008 Internship at the Laboratory of Immunology, Medical University Vienna, Vienna, Austria
Laboratory of Herbert Strobl, M.D.
Investigation of Langerhans cell behavior upon stimulation with different antigens

03/2009 – 05/2010 Diploma Thesis at the CHILDREN'S CANCER RESEARCH INSTITUTE, St. Anna Kinderkrebsforschung, Vienna, Austria
Laboratory of Peter Ambros, PhD
Heterogeneous *MYCN* amplification neuroblastoma - amplicons, genetic background, and genomic instability

Acknowledgements

First, I want to express my gratitude to Peter Ambros for giving me the opportunity to work on this interesting project which led to this diploma thesis, for his support along the way and for his confidence in me to handle the numerous conferences and meetings he sent me to. I also want to thank my colleagues in the lab, Inge Ambros for the fruitful discussions of my data, Bettina Brunner and Andrea Ziegler for the introduction to the different procedures, and Sabine Taschner-Mandl, Eva Bozsaky and Heidi Binder for their support and advice. I am also much obliged to Max Kauer for his help with the SNP array data visualization. Thank you to all the other wonderful people at the CCRI for the great working atmosphere.

A note of thanks goes also to the contributors outside of the CCRI, Tommy Martinsson and Jennie Erichsen for the SNP arrays, Tilmann Johannes and Rudolf Drescher for their help with the automatic microscope, and Reginald Bittner for his insights on the γ H2AX immunostaining. I also wish to thank Hans Rotheneder for being the supervisor of my diploma thesis at the University of Vienna.

Furthermore, I want to thank all my friends for their friendship and loyalty.

Last but not least, I owe my utmost gratitude to my parents and my siblings for their unswerving support, encouragement, and inspiration.